FACULTY OF INFORMATION TECHNOLOGY AND ELECTRICAL ENGINEERING

DEGREE PROGRAMME IN WIRELESS COMMUNICATIONS ENGINEERING

MASTER'S THESIS

Design and implementation of an uplink connection for a light-based IoT node

Author	Krystian Marcel Chorab
Supervisor	Prof. Marcos Katz
Second Examiner	Dr. Juha Häkkinen

June 2021

Chorab K. (2021) Design and implementation of an uplink connection for a light-based IoT node. University of Oulu, Faculty of Information Technology and Electrical Engineering, Degree Programme in Wireless Communications Engineering, Master's Thesis, 59 p.

ABSTRACT

In the wake of soaring demand for shrinking radio frequency (RF) spectrum, light-fidelity (LiFi) has been heralded as a solution to accommodate resources for future communication networks. Infrared (IR) and visible light communication (VLC) are meant to be used within LiFi because of numerous advantages. By combining the paradigm of internet of things (IoT) along with LiFi, light-based IoT (LIoT) emerges as a potential enabler of future 6G networks. With tremendous number of interconnected devices, LIoT nodes need to be able to receive and transmit data while being energy autonomous. One of the most promising clean energy sources comes from both natural and artificial light. In addition to providing illumination and energy, light can also be utilized as a robust information carrier. In order to provide bidirectional connectivity to LIoT node, both downlink and uplink have to be taken into consideration. Whereas downlink relies on visible light as a carrier, uplink approach can be engineered freely within specific requirements. With this in mind, this master's thesis explores possible solutions for providing uplink connectivity. After analysis of possible solutions, the LIoT proof-of-concept was designed, implemented and validated. By incorporating printed solar cell, dedicated energy harvesting unit, power-optimised microcontroller unit (MCU) and light intensity sensor the LIoT node is able to autonomously transmit data using IR.

Keywords: LIoT, VLC, IoT, Printed electronics, Infrared, Uplink, Indoor energy harvesting, Energy autonomous, 6G.

TABLE OF CONTENTS

FOREWORD

The aim of this thesis is to investigate uplink opportunities as well as devise a working prototype that could be integrated into already existing LIoT node. The research work was carried at the Centre for Wireless Communications (CWC), University of Oulu, Finland and funded under the 6G flagship program.

I would like to thank Prof. Marcos Katz for guidance, support and giving me leeway in shaping the thesis. I am thankful to Dr. Juha Häkkinen and Esko Strömmer from VTT Technical Research Centre of Finland for mutual brainstorming and pieces of advice that helped me advance steadily. Many thanks to Jari Sillanpää for swiftly placing orders and providing me with all the necessary equipment. Last but not least, Jasper Sikken, the man behind AEMSUCA harvester, deserves a token of my gratitude for all his help. Finally, I am grateful to Domantas Var for lending me a pack of resistors and to my Family for great support throughout the time spent in Oulu.

Oulu, 21st June, 2021

Krystian Marcel Chorab

LIST OF ABBREVIATIONS AND SYMBOLS

ACO-OFDM	asymetrically clipped optical orthogonal frequency division multiplexing
AP	access point
APD	avalanche photodiode
AWGN	additive white Gaussian noise
BER	bit error rate
BiCMOS	bipolar complementary metal-oxide-semiconductor
CAP	carrierless amplitude modulation
CMOS	complementary metal-oxide-semiconductor
CNN	convolutional neural networks
COB	chip on board
CSK	color shift keying
DC	direct current
DD	direct detection
DCO-OFDMA	direct current orthogonal frequency division multiplexing
DPPM	differential pulse position modulation
eU-OFDM	enhanced unipolar orthogonal frequency division multiplexing
EPPM	expurgated pulse position modulation
FFT	fast Fourier transform
FDD	frequency division multiplexing
FET	field effect transistor
IFFT	inverse fast Fourier transform
IoT	internet of things
IM	intensity modulation
IR	infrared
ISI	inter symbol interference
LED	light emitting diode
LCD	liquid crystal display
LiFi	light fidelity
LIoT	light-based internet of things
LMS	least mean square
LOS	line of sight
LS	living surfaces
LTE-A	long term evolution - advanced
MIMO	multiple input multiple output
MCU	microcontroller unit
MEMS	micro electromechanical systems
mMTC	massive machine type communication
MPPM	multipose pulse position modulation
MRR	modulated retroreflector
MTD	machine type device
MQW	multiple quantum well
NLOS	non line of sight
NOMA	non-orthogonal multiple access
NR	new radio

OEIC	optoelectronic integrated circuit
OFDM	orthogonal frequency division multiplexing
OLED	organic LED
OOK	on-off keying
OP-AMP	operational amplifier
OPPM	overlapping pulse position modulation
PAM	pulse amplitude modulation
PAPR	peak-to-average noise ratio
pc-LED	phosphor-converted LED
PD	photodiode
PE	printed electronics
PPM	pulse position modulation
PWM	pulse width modulation
PV	photovoltaic
RF	radio frequency
RGB	red, green, blue
RLL	run length limited
RLS	recursive least square
RMS	root mean square
SCFDE	single carrier modulation with frequency-domain equalization
SDN	software defined networking
SNR	signal to noise ratio
SOC	system on chip
SPAD	single-photon avalanche photodiode
SPAM	superposed pulse amplitude modulation
URLLC	ultra-reliable low latency communication
U-OFDM	unipolar orthogonal frequency division multiplexing
TIA	trans-impedance amplifier
WDD	wavelenght division multiplexing
WPT	wireless power transfer
VLC	visible light communication
VPPM	variable pulse position modulation
μLED	micro LED

1 INTRODUCTION

The area of wireless communication has been evolving steadily to satisfy the demand of the ever-growing number of users as well as more and more data-hungry services. Whereas the first generations of wireless technologies had been engineered solely to facilitate communication between humans the future ones are expected to make it possible to communicate not only for humans but also between devices such as computers, vehicles, sensors or drones themselves. This concept of providing wireless connections to various machine type devices (MTD) by means of internet infrastructure was termed internet of things (IoT). IoT is designed to enable a wide range of applications with various requirements in numerous aspects of life. In terms of 5G New Radio (NR), IoT can provide two kind of services: massive machine type communication (mMTC) and ultra-reliable low latency communication (URLLC). The former one ensures connectivity of a very large number of low-energy and low-data-rate devices and the latter requires very low latency and ultra-high reliability [1]. The predictions in IoT connections show a staggering growth from under a billion in 2017 to 3.9 billion by 2022 [2] and to 30 billion connections by 2030 [3]. This coexistence of such a whopping number of devices poses a multitude of challenges and risks associated with energy autonomy of nodes, cost-efficiency, energy consumption and privacy and security, to name a few. An attempt to handle these numbers by just relying on radio communications may prove unviable due to the increasing shared radio frequency (RF) spectrum shortage alias spectrum crunch. According to [4] the entire RF spectrum will be fully utilized around 2035 in the US. One of the most straightforward solutions to this problem is moving to different, possibly larger frequency bands that could accommodate the massive number of devices. In recent studies, light fidelity (LiFi) has emerged as a suitable candidate. It is an umbrella term for wireless technology using infrared (IR) and visible light communication (VLC). One major characteristic is that LiFi's unregulated and unlicensed spectrum (780 THz) is roughly 2600 times the size of the entire radio frequency spectrum (300 GHz) [5] which yields extremely capacious space for future applications and, moreover, is not affected by interference from radio systems and vice versa. LiFi boasts better physical layer security as the potential eavesdropper would have to be in a direct vicinity to the transmitted light beam. Additionally, LiFi can be used in sensitive environments where radio waves could disrupt the proper functioning of critical infrastructure [6]. Next, it was shown in [7] that a VLC can theoretically reach a data rate of 10 Gbps with single micro light emitting diode (μLED) and rates up to 5 Gbps with red, green, blue (RGB) LED. As regards the access to shared resources, authors in [8] proposed a non-orthogonal multiple access (NOMA) in VLC which is also envisioned to be part and parcel of 5G. Given the aforementioned arguments, there is every reason to believe that LiFi has enormous potential for becoming one of the 5G and 6G enablers.

With already existing LED lightning in indoor spaces, it would make the work of integration with other networks simpler, and by taking into account the dual nature of VLC which serves two purposes: communication and illumination, one can imagine the resultant energy savings [9]. Typically, a communication link is desired to be bidirectional, that is capable of exchanging data both in downlink and uplink directions. In wireless communication, there is a tendency that one end of the link is more powerful than the other. In the VLC-IoT scenario, the situation stays the same with a transceiver, whose size and power consumption is of secondary importance, being located in the ceiling

and IoT nodes devoid of much processing power and energy scattered in room beneath the LEDs. Thus, the most fundamental challenge arises - how to establish an uplink connection with limited energy available. Most research to date has focused particularly on the downlink approach while neglecting an uplink one which is, by all means, more challenging to work out. In the work [10], the author proposed and implemented a downlink approach together with a light-based IoT (LIoT) node with energy harvesting unit and taking advantage of printed electronics (PE) technology. Designing an energy-autonomous LIoT node by utilizing PE poses numerous challenges as PE technology is often subpar in terms of overall performance. For example, printed solar cells, despite being flexible and inexpensive, offer much less efficiency than conventional ones. Vast research has been done around energy harvesting technology which would allow an IoT node to power its circuit by means of renewable energy which may come from RF or thermal energy, ambient light or vibration. Designated chips have been developed to efficiently harvest, store and convert energy to power electronic components. In the future energy is expected to be harvested from many sources simultaneously. Authors in [11] designed hybrid energy harvesting system capable of feeding on both RF and solar energy. PE is an emerging technology that facilitates on-demand, quick production of extremely cheap and physically flexible electronic circuits which can be molded or bent to fit any surface [12]. The steady advancements in designing powerful harvesting chips and low power PE heralds the beginning of widespread presence of battery-less, autonomous IoT nodes that can be effortlessly deployed with much less environmental footprint.

1.1 The goal of the work

The goal of the master thesis is to study the possible solutions for an uplink communication between LIoT node and access point (AP) and design and implement a proof-of-concept. This work builds up on the master's thesis developed at CWC, University of Oulu, Finland [10]. The rest part of the thesis is organized as follows: In Chapter 2, an overview of VLC is presented. Chapter 3 explores possible pathways to incorporating uplink. Chapter 4 introduces the steps taken to design and implement the LIoT node which is then followed by evaluation of the system. The thesis is wrapped up in Chapter 6 and 7 that concern discussion, conclusion and future work.

2 OVERVIEW OF VISIBLE LIGHT COMMUNICATION

2.1 Basic VLC concept

VLC is a technique which takes advantage of visible light whose spectrum spans a range of 380 nm to 750 nm, which is equivalent to 430 THz and 790 THz, respectively. Visible light together with IR light are termed LiFi [13]. The spectrum of interest and the neighbouring ones are depicted in Figure 1. The aim of VLC is to provide simultaneous communication and illumination by means of already existing lightning infrastructure. LED is a key component and facilitator of VLC as it is capable of serving two functions at the same time: efficient, flicker-free lightning and transmitting modulated data. VLC is standardised by IEEE 802.15.7 [14] working group for wireless personal area networks.

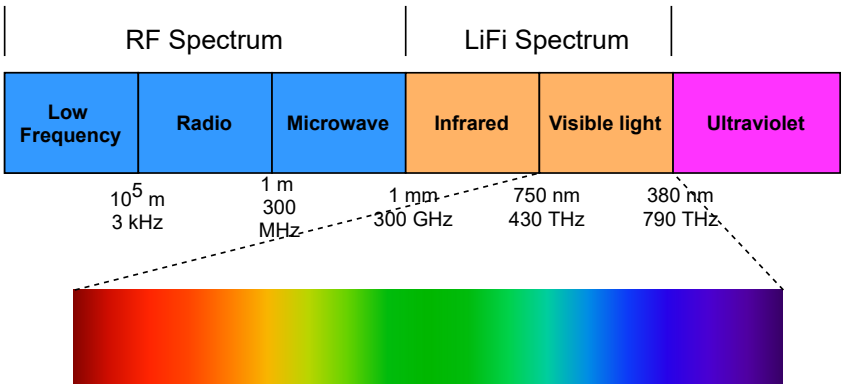

Figure 1. RF and LiFi spectra.

The VLC system architecture follows the same principles of any other radio communication scheme. First, the data is encoded in order to pre-equalize it against channel distortion and then modulated so as to pack as many information bits per bandwidth as possible with a view to increasing throughput. Such pre-processed data is fed into the driver that controls the output of the visible light emitter according to the modulated sequence. On the receiver side, the incident wave is captured by a detector which transforms the light wave into electrical signal which is then demodulated and decoded. The described flow is presented in Figure 2.

2.2 Transmitter

2.2.1 Light emitters

In VLC systems, LEDs are used as illumination and transmitter sources at the same time. To date, LEDs have evolved into multiple forms such as phosphor-converted LED (pc-LED), multi-chip LED, organic LED (OLED) and micro LED (μLED). Pc-LEDs and multi-chip LEDs are primarily and widely used as white light sources due to their low cost. They generate two or more different wavelengths to produce white light. The structure of pc-LED and multi-chip LED is depicted in Figure 3. The pc-LED emits white light by mixing short wavelength light with long wavelength light that comes

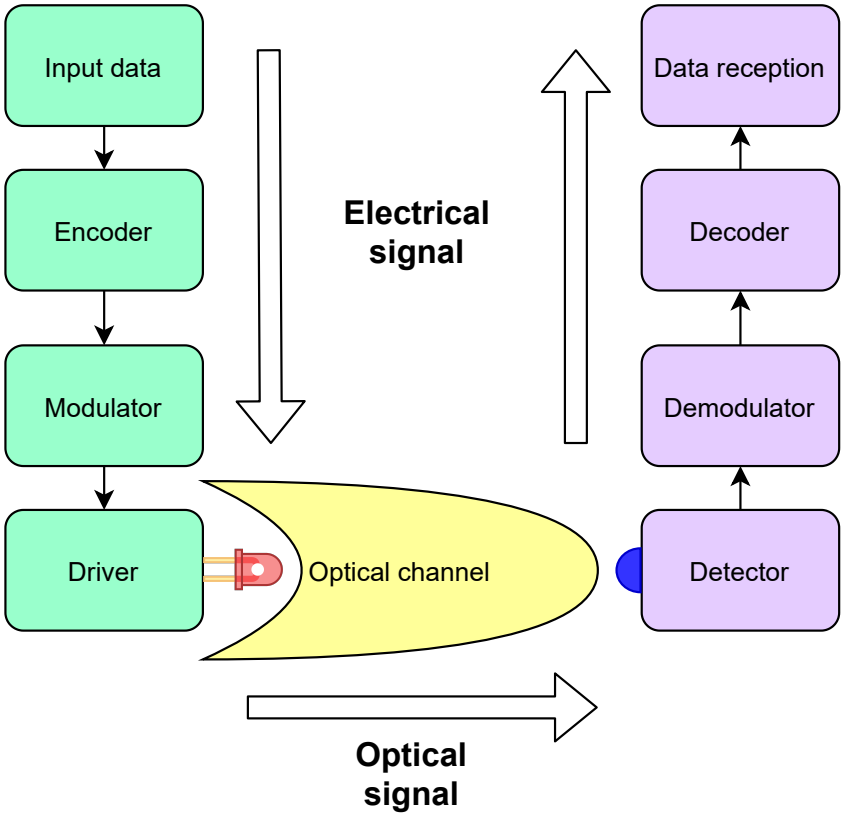

Figure 2. VLC system architecture.

through phosphor coating. This type of LED can achieve luminous efficacy of over 150 lm/W [15]. Nevertheless, owing to the slow relaxation time of the phosphor, pc-LEDs are subject to limited bandwidth of just several MHz [16]. Multi-chip LEDs produce the white light by mixing together different monochromatic lights for example red-green-blue LEDs. Higher cost and complexity notwithstanding, multi-chip LEDs are more preferred in communications because of their large intrinsic modulation bandwidth in comparison to pc-LEDs [17].

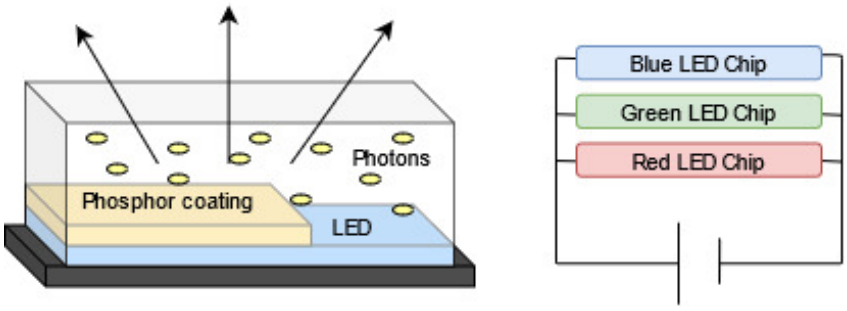

Figure 3. Pc-LED (left), Multi-chip LED (right).

LEDs have three fundamental constraints that are dimming control, chromaticity control and flicker-free communication.

Dimming control

Dimming is adjusting the brightness of LED by controlling the forward current. Spectral luminous efficiency function $V(\lambda)$ is defined to describe the fact that sensitivity of human eye to different wavelengths within visible spectrum varies. The perceived light power of transmitter LED measured in luminous flux is given by

$$\Phi = 683(lm/W) \int_{380nm}^{780nm} P(\lambda)V(\lambda)d\lambda, \tag{1}$$

where

$P(\lambda)$ denotes power spectral distribution, which represents the power of the LED at all wavelengths in the visible light spectrum.
Therefore, the luminous intensity is given by

$$I_t = \frac{d\Phi}{d\Omega}, \tag{2}$$

where

Ω denotes spatial angle.

One of the common approaches is digital dimming which uses pulse width modulation (PWM) where signal period is constant and dimming is achieved by proportionally changing the duty cycle.

Chromaticity control

Chromaticity control applies to multi-chip LEDs for which it is vital to show the quality of color irrespective of its luminance. Standard IEEE 802.15.7 adopted a method called color shift keying (CSK) which guarantees a real color representation.

Flickere-free communication

It is crucial for VLC LEDs to maintain a constant output power which corresponds to stable brightness, because long-term exposure to flickering light was proven to be detrimental to humans' well-being and can even pose health hazards. In order to avoid this phenomenon, the average light intensity should not fluctuate which means that signal should be direct current free (DC-free). The most common way is to employ run length limited (RLL) coding such as Manchester or 4B6B. They make sure that long runs of 1's and 0's do not occur which may cause flickering and clock recovery issues [18 p.27].

2.2.2 LED driver

According to [19], embedding information in phase or amplitude is not possible in VLC and the data has to be encoded by varying the intensity of light by direct modulation techniques which are simple and robust. In direct modulation, the modulated message signal is superimposed on the bias current which modulates the LED. This technique is presented in Figure 4.

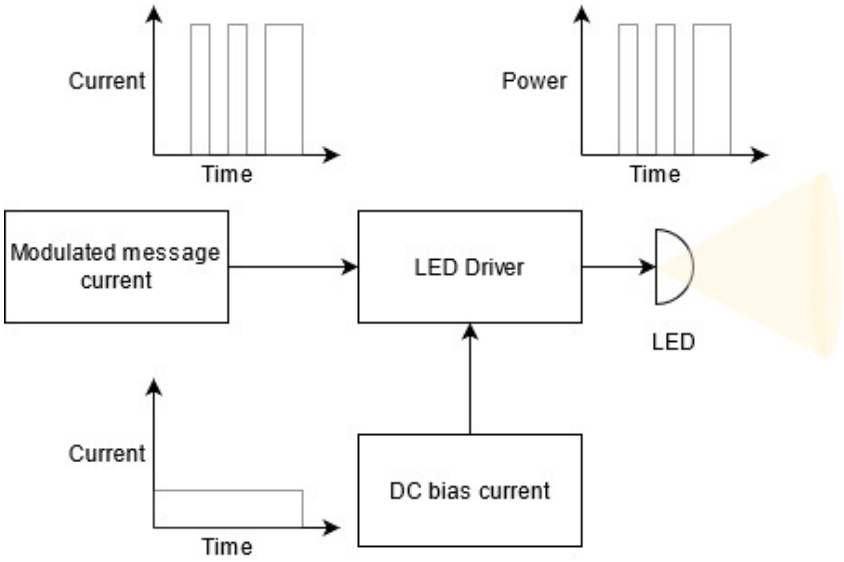

Figure 4. LED Driver.

The parameter that describes the ability of a receiver to detect optical signal is modulation depth which is expressed as follows

$$m = \frac{\Delta I}{I_0}, \tag{3}$$

where

ΔI denotes difference between peak and bias current,
I_0 denotes bias current.

2.3 Receiver

Optical receiver's role is to detect the incident wave, transform it into electrical signal and perform demodulation and decoding.

2.3.1 Detection unit

Detection unit refers to the front-end part of receiver which serves as an antenna in RF receivers.

Photodiode

A photodiode is commonly used in detection in VLC to convert the optical signal to the electrical one. Upon absorbing a photon with sufficient energy by the photodiode, an electron-hole pair is being created. In case when photodiode is driven by the

reverse voltage holes head for the anode and electrons for the cathode, thus generating photocurrent.

Photodiodes can be dividied into PN photodiode, PIN photodiode and avalanche photodiode (APD). PN photodiodes' cutoff frequency is around 100 - 200 MHz. With PIN photodiodes's additional layer called intrinsic region cutoff frequency increases to the order of GHz. APD photodiodes boast very high sensitivity by incorporating the impact ionization process. APDs have been successfully implemented in optoelectronic integrated circuit (OEIC). With APDs' large diameter authors in [20] achieved sensitivity equal to -31.8 dBm at 1 Gbit/s using 0.35 μm complementary metal-oxide-semiconductor (CMOS) technology for a 200 μm diameter APD and very recently in [21] sensitivity of -33 dBm at 1 Gbit/s was reported with 800 μm diameter APD integrated in 0.35 μm bipolar CMOS (BiCMOS) receiver. Avalanche diodes which are biased considerably over the reverese-bias breakdown voltage are called single-photon avalanche diodes (SPAD). There are three parameters that describe photodiode: absorption coefficient, quantum efficiency and responsivity. Absorption coefficient is expressed as the received radiant flux Φ_r and when the attenuation is uniformly distributed can be written as

$$\Phi_r = \Phi_t e^{-\alpha d}, \tag{4}$$

where

Ω_t denotes radiant flux falling onto the photodiode's surface,

α is the linear attenuation coefficient dependant on the material and wavelength and

d is the thickness of the photodiode.

Next, photodiode's efficiency is represented by quantum efficiency which describes a ratio between the number of photocurrent's charge carriers and the number of photons penetrating into the surface of the photodiode. Lastly, responsivity defined in units of amperes per watt of radiant power is a measure similar to qunatum efficiency but also depends on incident wavelength [18 p. 28 - 29].

Imaging sensor

It was pointed out in [22] that imaging sensor or camera sensor can be used as visible light receivers. One advantage of this solution is that most of today's devices are equipped with some sort of camera sensor with matrices of minute photodetectors that could potentially turn them into VLC receivers. However, the high number of photodetectors makes it difficult to achieve high data rates and currently the throughput is limited to just a few kbps.

2.3.2 Receiver unit

The PD-based receiver architecture is shown in Figure 24. The optical signal, after being converted into photocurrent, needs to be again converted into voltage to facilitate processing using voltage-based methods. A trans-impedance amplifier (TIA) does the aforementioned function. Authors in [23] have designed and simulated the TIA for high-band VLC by exploiting a commercially available operational amplifier (OP-AMP).

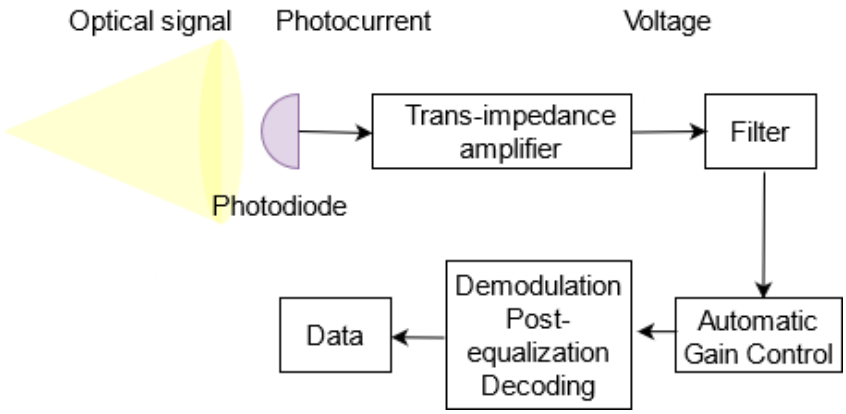

Figure 5. PD-based receiver architecture.

Next, the signal has to be filtered of noise components, which greatly decrease the performance of the VLC system. The ambient noise in the VLC stem mostly from artificial lightning, sunlight and reflections. To date, four methods of ambient light noise mitigation were proposed: optical filtering, frequency-domain filtering, encoding filtering and adaptive filtering whose traditional algorithms include least mean square (LMS) and recursive least square (RLS). Over the past decade filtering algorithms based on artificial neural networks were investigated [24, 25]. However, they concerned only traditional wireless networks. In [26], authors designed and implemented adaptive filtering for VLC based on convolutional neural networks (CNN) boasting 40% lower bit error rate (BER) than that of LMS. Once amplified, noise-free signal is equalized, demodulated and decoded.

2.4 Optical channel

2.4.1 Propagation link

The propagation link can be divided into two categories. One is based on the existence of direct path between transmitter and receiver and the other on directionality between them. The former category distinguishes a line-of-sight (LOS) path and non-line-of-sight (NLOS) path. The latter classifies links into three categories: directed, non-directed and and hybrid links Therfore, six examples of different link configurations are presented in Figure 6.

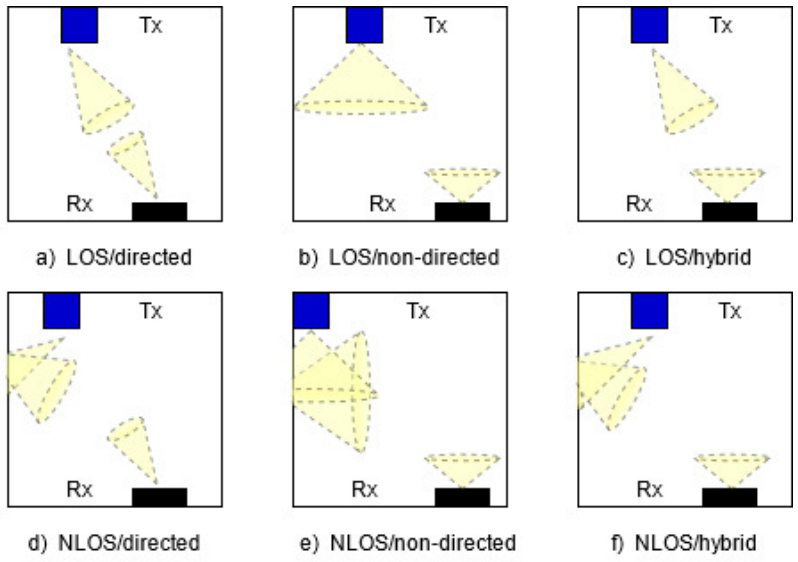

Figure 6. Classification of the propagation links. Recreated from [18 p. 30].

The highest power efficiency can be achieved by ensuring LOS and directed link at the same time. However, NLOS conditions improve the robustness of the wireless system since photodiode is usually able to detect signals from reflected paths. Additionally, according to [18] multipath fading does not exist in VLC on account of the physical photosensitive area of a photodiode which is by far larger than the square wavelength of the light.

2.4.2 LOS link

Luminous flux introduced in (2) represents the total optical power generated by the light source and takes into account the human eye response. In case the light does not affect humans it is more convenient to use radiant flux which is also the total emitted light and can be obtained by measuring and integrating each wavelength emitted by LED. Next, another useful measure indicating the intensity of light coming from the front of LED within a coned shape sector of the total space around the light source is radiant intensity which is not dependant on the distance. Its unit is Watt/steradian (W/sr) and the formula goes as follows

$$R(\theta) = \frac{m+1}{2\pi} cos^m(\theta) P_{LED}, \tag{5}$$

where

P_{LED} denotes the total radiated power given by $P_{LED} = \int_\lambda P(\lambda) d\lambda$,
$P(\lambda)$ denotes the spectral power distribution,
θ denotes the angle between the emitted light and the normal to the LED surface,
and m denotes the order of Lambertian emission defined as

$$m = \frac{ln2}{ln\, cos(\Phi)_{1/2}}, \tag{6}$$

where

$\Phi_{1/2}$ denotes the half-power angle.

Then by dividing the radiation intensity by the squared distance one obtains irradiance

$$E_e(d) = \frac{R(\theta)}{d^2}. \tag{7}$$

In order to obtain the received power, one should consider the photodiode's effective photosensitive area $A_e(\psi)$ defined as

$$A_e(\psi) = Af(\psi)cos(\psi), \tag{8}$$

where

A denotes photodetector physical area,
ψ denotes the incident angle,
and $f(\psi)$ denotes the optical filter gain.

Now, the received power is

$$P_r = E_e(d)A_e(\psi). \tag{9}$$

and the path loss or DC gain is given by

$$H_{LOS} = \frac{(m+1)A}{2\pi d^2} cos^m(\theta) f(\psi) cos(\psi). \tag{10}$$

2.4.3 NLOS link

The NLOS signal can reach the receiver after many reflections from the nearby walls and objects. The DC gain after the first bounce is expressed as

$$H^1_{NLOS} = \int_s \frac{(m+1)A}{2\pi^2 d_1^2 d_2^2} \gamma cos^m(\theta_1) cos(\theta_2) f(\psi) cos(\psi_1) cos(\psi 2) dA_s, \tag{11}$$

where

d_1, d_2 denote distances of paths,
γ denote spectral reflectance,
and $\theta_1, \theta_2, \psi_1, \psi_2$ denote irradiation and incident angles, respectively.

2.4.4 Noise

Various noises decreasing the system's performance can be distinguished in VLC. Some types of noise such as background radiation noise are more dominant and affect the received signal-to-noise ratio (SNR) more dramatically than the quantum noise for example. A brief description of noises types follows.

- Quantum noise is spurred by the fluctuating photons from the optical source whose number follows a Poisson distribution. It invariably appears to be shot noise due to the frequently used intensity modulation.
- Background radiation noise is the major contributor of noise in VLC systems and is caused by ambient light photons which come from various lamps and sun and are collected by the photodiode. Interestingly, because of its high intensity ambient light noise can be modelled as additive white Gaussian noise (AWGN).
- Thermal noise is due to the random fluctuation of electrons in any conducting material and is proportional to the temperature.
- $1/f$ noise is non-white low frequency noise present in many areas of life such as music, biology, electronics and even economics.[27] It can degrade performance in precision measurement applications.
- Dark current noise exists in the photodiode even in the absence of incident light and is related to the temperature of the photodiode and the bias voltage.

2.4.5 Receiver SNR

In [22], authors proposed calculating the received SNR as

$$SNR = \frac{P_R^2}{\sigma_{shot}^2 + \sigma_{thermal}^2}, \tag{12}$$

where

P_R denote received power,
σ_{shot} and $\sigma_{thermal}$ denote standard deviation of shot and thermal noise.

Background radiation noise was not included in the above formula since its impact is supposed to be mitigated by means of high pass filter in the receiver and the shot and thermal noise come from photodetector circuitry. Another approach was chosen in [28], in which authors performed a analysis of a VLC link budget. The received power was calculated by multiplying the transmit power by the path loss and then represented by the root-mean-square (RMS) value of photocurrent

$$I_{PD} = \frac{1}{2} PL \int_{\lambda} S_t(\lambda) R_{PD}(\lambda) d\lambda, \tag{13}$$

where

PL denotes the path loss,

S_t denotes spectral power distribution,
and R_{PD} denotes responsivity of PD.

The receiver noise was calculated as a sum of four sources of noise: PD, TIA, high-pass filter and power supply. The resulting SNR was calculated as follows

$$SNR = \frac{(I_{PD} - I_{min})^2 Z_{TIA}^2}{V_{n\_tot}^2}, \tag{14}$$

where

I_{min} represents the threshold current,
Z_{TIA} denotes transimpedance gain of the TIA,
and V_{n_tot} denotes the sum of noises.

2.5 Modulation schemes

The most prominent characteristic of VLC modulation methods is that neither phase nor amplitude can be modulated or detected by means of LEDs and PDs [29]. This means that traditional RF modulation methods should be well rethought before applying them to VLC. In VLC techniques regarding modulation and detection the light wave are termed intensity modulation/direct detection (IM/DD). In [30, 31], authors presented a detailed overview of modulation methods for VLC. Generally, literature indicates three types of modulation which are presented briefly in the forthcoming subsections.

2.5.1 Single carrier/Carrierless modulation

The first group of single carrier modulation scheme encompasses pulse modulation methods, namely pulse amplitude modulation (PAM), pulse position modulation (PPM) and pulse width modulation (PWM). PAM is the most commonly used modulation type in VLC with a simple on-off keying (OOK) being a particular, two-level example widely embraced and adopted in the IEEE 802.15.7 standard. Different variations of these methods were conceived in order to tackle issues which have already existed in conventional RF systems or are VLC-specific only. Inter-symbol interference (ISI) can be tackled for example with single carrier modulation with frequency-domain equalization (SCFDE) and the solution to LED nonlinearity being a challenge for PAM systems can be superposed PAM (SPAM). In an orthogonal PPM, one symbol duration is equally divided into N time slots and only one of the N slots is used for transmission. Therefore, intensity is not used to represent the data but the position of the pulse indicates the transmitted bits. PPM needs less average power as opposed to PAM but at the expense of increased bandwidth and peak-to-average power ratio (PAPR). In order to increase the limited spectral efficiency of PPM numerous alterations were proposed such as differential PPM (DPPM), multipulse PPM (MPPM), overlapping PPM (OPPM), expurgated PPM (EPPM) and variable PPM (VPPM). Carrierless amplitude and phase modulation (CAP) has gained interest of researchers as a promising modulation scheme for VLC on the

grounds that it combines high spectral efficiency, low PAPR and simple implementation [32].

2.5.2 Multicarrier modulation

Orthogonal frequency division multiplexing (OFDM) is a popular multiple access technique employed for instance in Long term Evolution-Advanced (LTE-A) standard [33]. However, conventional OFDM produces complex, bipolar signals that are not suitable for IM/DD that require the amplitude of the signal to be real and non-negative.

The starting point in transforming the traditional OFDM is a DC-biased optical OFDM (DCO-OFDMA) where optical OFDM is modulated on the intensity of light and forced to be unipolar and real-value. The block diagram of the DCO-OFDM system is illustrated in Figure 7.

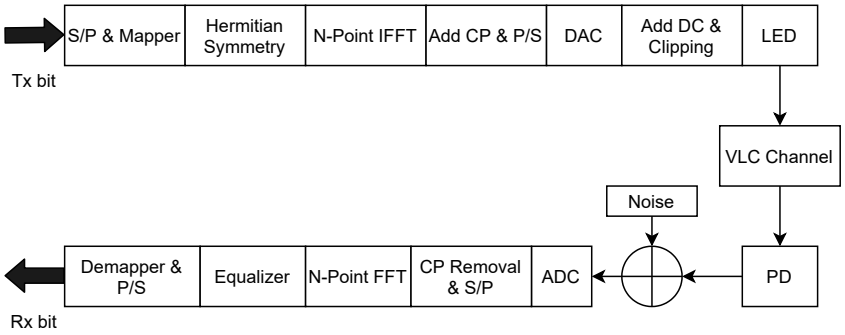

Figure 7. The block diagram of DCO-OFDM communication system. Recreated from [18 p.91].

In the above diagram S/P and P/S denote serial to parallel and parallel to serial, respectively. FFT denotes Fast Fourier Transfrom and IFFT inverse FFT. CP means cyclic prefix and DAC and ADC are digital to analog and analog to digital converter. One disadvantage of this scheme is its inherent low power efficiency due to the need of high DC bias. Asymetrically clipped optical OFDM (ACO-OFDM) and PAM discrete multitone (PAM-DMT) were developed to fix the issue of power efficiency compromising the spectral efficiency by replacing some subcarriers with clipping distortions. The last type of OFDM dubbed unipolar OFDMA (U-OFDM) does not require clipping operations and the block length is increased to accommodate the negative amplitudes. The state-of-the-art enhanced U-OFDMA (eU-OFDM) was investigated in [34] and promises to deliver considerable energy savings in high spectral efficiency configurations at the cost of higher computational complexity.

2.5.3 Multicolor modulation

Multicolor modulation is possible only with RGB LEDs where three color leds are used to generate the signal. In Figure 8 scrambler makes sure that communication is flicker-free. Then, after channel coding color coding block maps bits into coolor coordinates (x, y)

which are later transformed to intensity vector $[P_i, P_j, P_k]$ which modulates three light sources operating in seven different bands within visible spectrum.

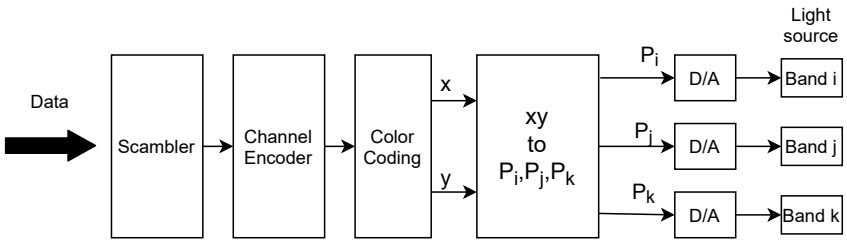

Figure 8. The block diagram of CSK transmitter. Recreated from [18 p.148].

By denoting the color coordinates of the three light sources as $(x_i, y_i), (x_j, y_j), (x_k, y_k)$ one can calculate their intensities as

$$x_p = P_i x_i + P_j x_j + P_k x_k, \tag{15}$$

$$y_p = P_i y_i + P_j y_j + P_k y_k, \tag{16}$$

$$P_i + P_j + P_k = 1 \tag{17}$$

CSK can be combined with DCO-OFDM in order to increase the data rate while maintaining the CSK's non-flickering property [35].

2.6 LIoT concept incorporating PE

LIoT is a futuristic paradigm featuring an abundance of low-cost, energy-autonomous nodes that utilize the LED lightning infrastructure both for energy harvesting and communication. The connection to internet can be seen as an "Expose-and-Connect" approach. Every time the node is exposed to light it is connected to internet. Together with an up-and-coming PE technology LIoT nodes can be conveniently and cheaply placed on various surfaces. This combination paves the way for many applications such as smart product labelling, interactive logistics, patient monitoring or indoor positioning. Figure 9 illustrates the overall LIoT concept including the LIoT node and the VLC access point (VLC AP). VLC Access point is both the transceiver and light (energy) provider for the LIoT node. Downlink encompasses solar energy in the form of light and data and uplink consists only of data send by LIoT node. Incorporating PE in the design of the LIoT node is likely to bring many desirable features from IoT perspective such as low price per node, quick and easy deployment, flexibility in design and ultra low energy consumption. The ultimate goal is to manufacture a LIoT node made of only printed components.

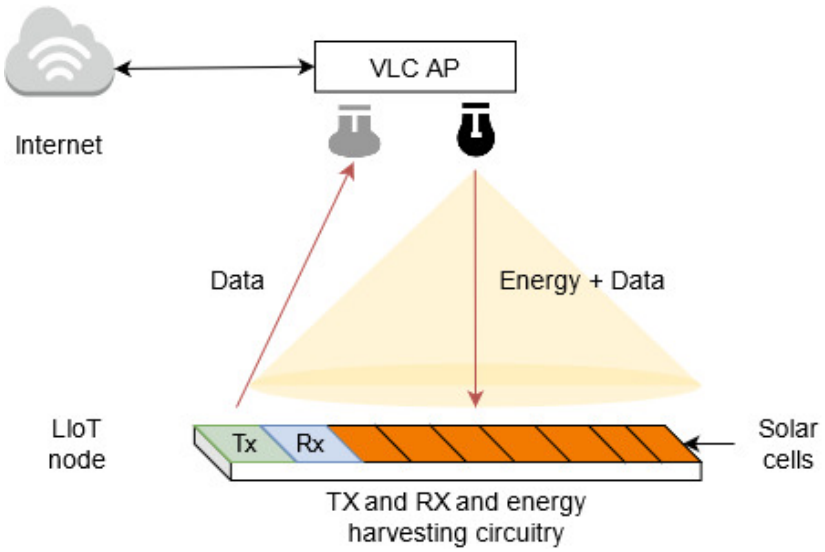

Figure 9. LIoT concept.

An extension of the LIoT concept is termed Living Surfaces (LS) where any large surface can be accommodated to have numerous functionalities such as as energy scavenging, energy storage, sensing, processing, displaying information and at the same time being wirelessly connected to other LIoT nodes/surfaces and internet [36].

2.7 Introduction to downlink system

The downlink VLC system was successfully designed and implemented in [10]. The transmitter part consists of Arduino Uno microcontroller (MCU), LED driver and chip-on-board (COB) LED array. The data generated in computer in MATLAB is modulated using PPM and data frames were based on RECS-80 protocol. A photodiode-based receiver with Arduino Pro Mini MCU together with energy harvesting unit and photovoltaic (PV) cells was developed and tested. Two types of PV cells were tested for performance comparison: printed Perovskite cells developed by Technical Research Centre of Finland (VTT) and printed organic PV cells crafted by Infinity PV. Also, the benefit of using energy harvesting unit was confirmed for two types of displays: e-ink based and electrochromic based. The BER performance was evaluated for both window sunlight and indoor artificial lightning for the maximum link distance of 0.6 m.

3 LIOT COMMUNICATIONS IN UPLINK: PROSPECTIVE APPROACHES

Whereas most of efforts have been focused on downlink in VLC and on increasing the data rate at rather short distances investigating uplink approach appears to have been somewhat neglected. Establishing a bidirectional link is one of the biggest challenges and poses numerous issues that vary depending on application. The fundamental principle of VLC node is that it is supposed to be battery-free and should rely on energy harvested from the environment only. This renders the node to perform only essential computations and whose energy consumption is optimised. Problems faced in energy-constrained VLC node support the advancements in wireless power transfer (WPT) [37]. In Figure 10, VLC AP is usually installed on the ceiling in a typical indoor office scenario. The red arrow indicates the uplink direction to be considered in the thesis. The VLC AP has constant power supply and preferably highly sensitive receiver. A stationary or non-stationary VLC node resides in the direct illumination area and receives the incident light which both contains modulated data and serves as an energy source to power the device. Using the available, harvested energy the node should be able to receive, demodulate and decode the transmitted signal and perform the inverse steps to transmit its own data towards the VLC AP.

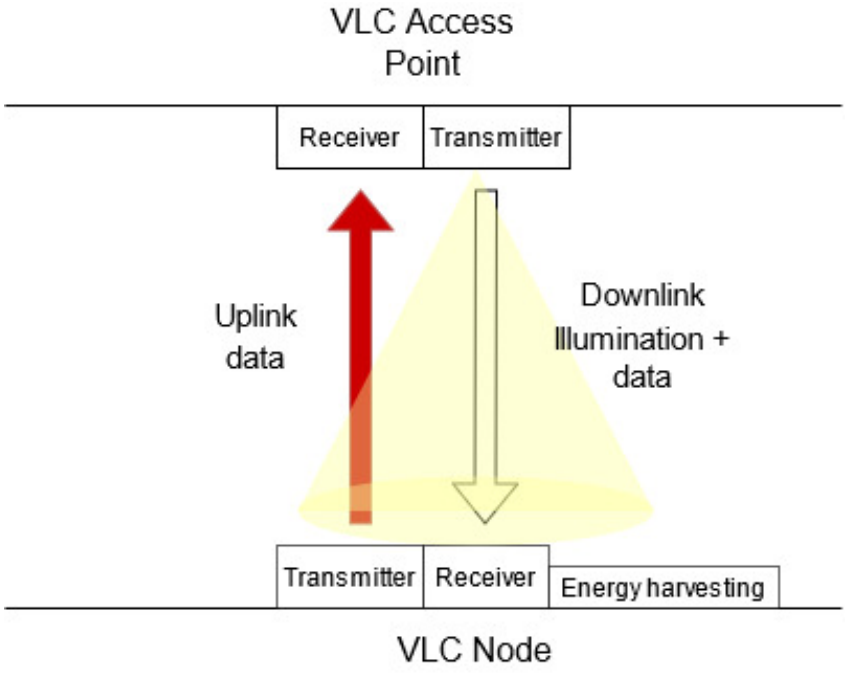

Figure 10. VLC bi-directional communication system.

The forefront uplink solutions that have been proposed in the literature include WiFi-VLC known as hybrid VLC, infrared (IR) light and retroreflection. The WiFi-VLC typically combines visible light for downlink and RF for uplink using the WiFi standard and has been researched extensively. WiFi-VLC performance has been enhanced with software-defined networking (SDN) [38], reinforcement learning [39] and multiple-input multiple-output (MIMO) technology [40]. Also, advanced joint resource management

algorithm was presented for WiFi-VLC hybrid networks [41]. Since hybrid VLC is not a pure VLC technology and partly contradicts the philosophy of abandoning RF spectrum it will not be covered in this work.

3.1 Uplink based on infrared light

The uplink approach using IR has been entrenched in research as the most suitable technology. One way of avoiding large self-interference at the transceiver due to cross-talk between the incident and emitted light is wavelength-division duplexing (WDD) being the equivalent of frequency-division multiplexing (FDD) in RF. It employs non-overlapping frequency bands for downlink and uplink. In case of IR approach, downlink employs visible spectrum and uplink infrared spectrum thus being invisible to human eye and simultaneously not posing any threat related to detrimental effect of flickering. Lastly, IR diodes and PDs and relevant circuitry are cheap and commercially available. In [42], authors demonstrated the first practical bi-directional optical link exploiting IR LED for uplink and achieving data rate between 100 and 250 Mbit/s at the distance of 2m and BER lower than 10^{-3}. In addition, a high angle tolerance at the receiver was confirmed which means an increased mobility of the VLC node. A low data rate uplink transmission of 45 bps can be established using IR LED and a commercial surveillance camera - picamera which is able to detect infrared light [43]. It was shown in [44], after establishing a bi-directional link with compact hardware capable of supporting 100 kbps at the distance of 1 m, that cross-talk can be mitigated by a proper alignment of transmitter and receiver. An uplink transmission was simulated to achieve a data rate of 3.57 Gbit/s using OOK and an optical hologram in front of transmitter together with four branches angle diversity receiver (ADR) which provide beam steering and ISI reduction [45]. An important issue of IR uplink transmission with link blockage and random device orientation was investigated in [46] and closed-form expressions for the statistics of uplink channel under the aforementioned conditions were proposed. One downside of infrared uplink, however, is the fact that generally diodes consume most of the available energy. One solution may be to substitute traditional IR diode with a printed one. Nevertheless, printed IR diodes have not been yet crafted to the point of being useful in any prototyping due to their extremely low performance.

3.2 Uplink based on retroreflection

Retroreflection is a phenomenon when an incident wave is reflected (backscattered) exactly in the opposite direction it came from, regardless of the changes in position of the source. It is guaranteed by the special alignment of reflective surfaces which can either be orthogonal or spherical, which is illustrated in Figure 11. A real example of corner-cube retroreflector is shown in Figure 12. Retroreflectors can be configured to work as passive or active devices. In a passive mode, it only reflects the interrogating wave without modifying it, thus allowing to calculate the round-trip time. Such approach can be found in applications where accurate range measurements are required. In an active mode, the retroreflector together with integrated modulator perform modulation of the incident wave before returning it to the source. These are modulated retroreflectors (MRRs).

Since establishing an uplink communication by means of retroreflection does not require any active signal generation and transmission at the VLC node it appears to be suitable for low-power communication that VLC is aiming at. Additionally, retroreflection yields extra security to uplink channel due to narrow beam that can only be eavesdropped by intercepting the direct beam. This advantage may also be perceived as a disadvantage at the same time since generally retroreflective communication must have a LOS link in order to backscatter the incident wave directly towards the VLC AP.

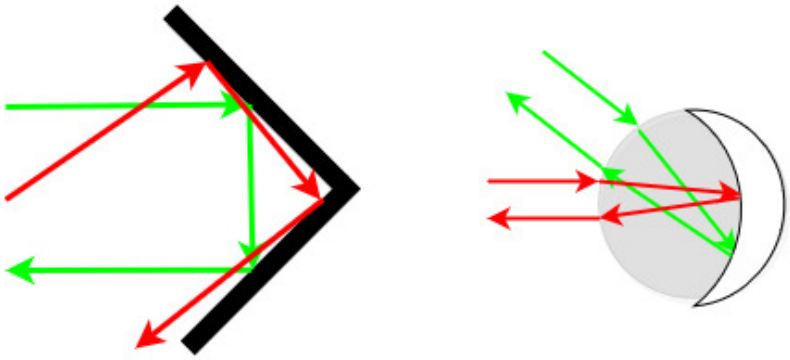

Figure 11. Types of retroreflectors: corner-cube (hollow) (left), spherical (cat's eye) (right).

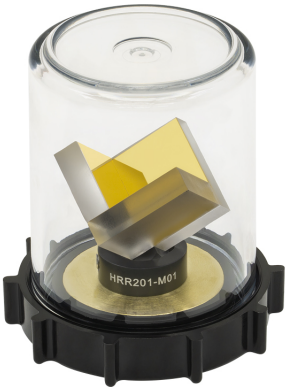

Figure 12. Hollow retroreflector mirror developed by Thorlabs [47].

However, the lack of an active uplink transmission may require higher transmitter output power at the VLC AP since the received SNR at VLC AP and link distance are determined by the strength of the transmitted beam. The power received at the VLC AP can be expressed as [48]

$$P_r = P_t - L_{downlink} - L_{uplink} - L_{rr} - L_{rx}, \tag{18}$$

where

P_t denotes transmited power,

$L_{downlink}$ denotes downlink path loss,
L_{uplink} denotes uplink pathloss,
L_{rr} denotes retroreflector efficiency,
L_{rx} denotes receiver losses such as coupling to the PD.

Thus far, three ways of modulating the incident wave have been reported and are described below. The principle stays the same for all of them and is based on placing a modulator either in front of or at the bottom of a retroreflector so that the incident wave can penetrate it upon reflection. Then, by deforming the modulator or changing its transparency it is possible to embed information onto the reflected light wave. This idea is presented in Figure 13.

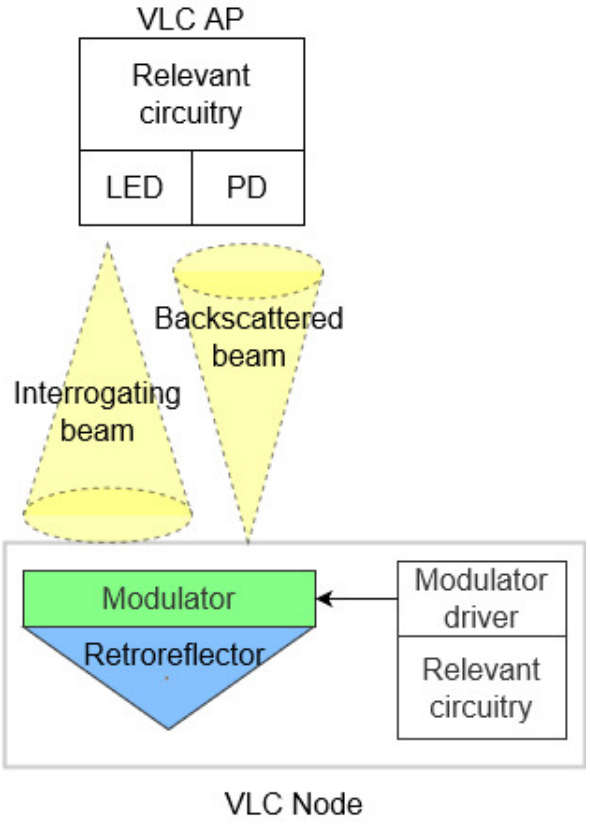

Figure 13. The retroreflective based uplink system architecture.

LCD shutter based modulation

Due to commercial availability, low price, relatively fast switching speed and power consumption of tens of μW liquid crystal displays (LCDs) have been leveraged as modulators in research. In addition, LCD can have large dimensions which may translate into larger area for solar cells or retroreflectors that can be mounted on the walls. LCDs are capable of passing or blocking light when electrical field, which controls the arrangement of liquid crystal molecules to polarize the light, is applied. Therefore, by toggling the LED it is possible to adopt an OOK modulation. In RETRO [49] LCD shutter was installed on a corner-cube retroreflector in IoT node to bounce back and

modulate the incoming wave. By so doing, it was possible to distinguish the reflected light for different IoT nodes and allow VLC-based, real-time localization. This approach was also used in [50] where authors explored uplink throughput enhancement by incorporating three separate pixels each with retroreflector and LCD shutter. This configuration facilitates the use of multi-level PAM such as 4-PAM or 8-PAM. LCD shutter adopting OOK was also implemented in an extensive, advanced system called Retro-VLC [51]. A compact, battery-free VLC node called ViTag shown in Figure 14 employs a simple retroreflective tape that is widely used in safety clothing and protective workwear. The system was shown to be capable of supporting 10 kbps downlink and 0.5 kbps uplink over a distance of 2.4 m.

Figure 14. The ViTag node in the Retro-VLC system $8.2cm \times 5.2cm$.

The aforementioned solution was upgraded by authors in [52] achieving uplink data rate of 1 kbps. This increase was a result of replacing Manchester coding with Miller coding and incorporating trend-based modulation together with code-assisted demodulation. It was noticed that even a small change in LCD transparency can be leveraged to carry information without the need of toggling LCD completely on and off which consumes more power and induces modulation delay.

Electrochromic display based modulation

One promising yet uncharted approach may be to substitute LCD shutter with electrochromic display. Electrochromism is a phenomenon of a material being able to change its optical properties through chemical reduction or oxidation when voltage is applied [53]. Electrochromic displays boast numerous advantages from the IoT point of view that are listed in Table 1.

Table 1. Pros and cons of electrochromic displays.

Advantages	Disadvantages
Non-light emitting	Slow switching time
Ultra-low power consumption	Low contrast
Free-form and flexible	
Easily printable	
Lightweight and thin	
Transparent	
Semi-bistable	
Environment-friendly	

A formidable obstacle in achieving data rates similar to the ones in LCD based modulation is very low switching speed. Despite consuming considerably less energy the most advanced printed electrochromic displays are able to change its state every 1 s at most. However, switching speed can be increased by altering the saturation limits of the on/off states.

MEMS based modulation

Micro-electromechanical systems (MEMS) offer another way of cooperating with retroreflector in order to modulate and backscatter the light wave. MEMS is a an umbrella term for miniaturized electromechanical elements that are manufactured by means of microfabrication. The building blocks of MEMS are MicroSensors, MicroActuators, MicroElectronics and MicroStructures [54]. In [55], a deformable MEMS mirror was crafted and used as a modulator. The mirror was placed behind the retroreflector so that the incident light first impinges on the surface of retroreflector and then bounces back from the mirror's surface which changes between two states: a flat state (off) and a corrugated (deformed) state (on). The former one which reflects most of the power to the source requires no power to maintain and the latter which creates a diffraction grating effect spreading the returned beam out of the direct reflection path needs just μW. The process responsible for switching between two states is called electrostatic actuation and occurs when voltage is applied to the conductive silicon substrate layer and reflective deformable gold mirror layer spurring an electrostatic force which deflects the flexible mirror surface. What is more deformable mirrors are claimed to be easily manufactured in standard semiconductor fabrication process.

MQW based modulation

Multiple-quantum-well modulation have not been yet widely investigated in VLC but it can potentially be combined with retroreflector and work similarly to previous solutions. In this method, a thin layer made of many quantum well modulators that can be modulated at very high frequencies is placed on a retroreflector. Quantum wells are based on quantum-confined Stark effect and change their absorption spectrum when electric field is applied. Fabry-Perot MQW were reported to be capable of being integrated with cat's eye retroreflector [56].

3.2.1 VLC node energy harvesting

Usually in order to harvest energy from ambient light in VLC and maintain battery-free operation one needs solar cells, an energy storage unit and a power management system. Solar cells convert optical energy into electrical energy through photoelectric effect that is stored in e.g. supercapacitor. One novel approach to energy harvesting and compact design was proposed and modelled in [57] where corner-cube retroreflector along with suitable modulator is deposited with a thin film of alkali metal. Alkali metals such as sodium (Na), potassium (K), rubidium (Rb) and caesium (Cs) are proved to free up electrons easily and thin film made of these metals boast high photoelectric efficiency. The formula to estimate the harvested power goes as follows

$$P = E_{lux} \times I \times A \times E_{solar}, \tag{19}$$

where

E_{lux} denotes the conversion rate from lux to $watt/cm^2$,
E_{solar} denotes solar cell power conversion efficiency,
I denotes illumination in lux,
A denotes solar cell area.

A tentative evaluation of the above formula with realistic values:

- $I = 300$ lux for indoor environment,
- $A = 25\, cm^2$,
- $E_{lux} = 1.46 \times 10^{-7}\, watt/cm^2/lux$ [58],
- $E_{solar} = 20\%$,

results in harvested power equal to $P = 219\, \mu W$ [50].

A careful design has to be taken into consideration when devising VLC node to minimise the power consumption so that the harvested energy is able to power the device and provide power autonomy. In [51], VLC node (ViTag) was equipped in the following energy efficiency enhancing solutions:

- Abstaining from ADC and performing most of processing in analog domain. Instead of ADC a comparator was chosen to digitailize the signal.
- In case of no incoming data MCU sleeps and when it receives data is works for only 8% of the receiving cycle.
- All transistors are set to operate at the lowest DC operating point nearing a cut-off state.
- As LCD consumes 70% of the power during transmission an energy reuse module was designed to save the current wasted during LCD charging and discharging.

It was observed that replacing bipolar transistors with field-effect transistors (FET) would potentially provide better energy efficiency. With these modifications the total energy consumed by the VLC node was measured to be 234 μW under 2.6 V operating voltage.

4 DESIGN AND IMPLEMENTATION OF A LIOT NODE FOR UPLINK COMMUNICATIONS

The prototype consists of transmitter and receiver units. The former was designed as LIoT node and the latter as an access point. The LIoT node is intended to work under low-power regime and be entirely autonomous. The uplink transmission was realized using IR and the transmitted data comes from light intensity sensor.

4.1 LIoT Node - Transmitter

The building blocks of LIoT transmitter are shown in Figure 15. The main task for the LIoT node is to transmit readings from light intensity sensor at arbitrary interval using infrared light and remain energy autonomous at the same time.

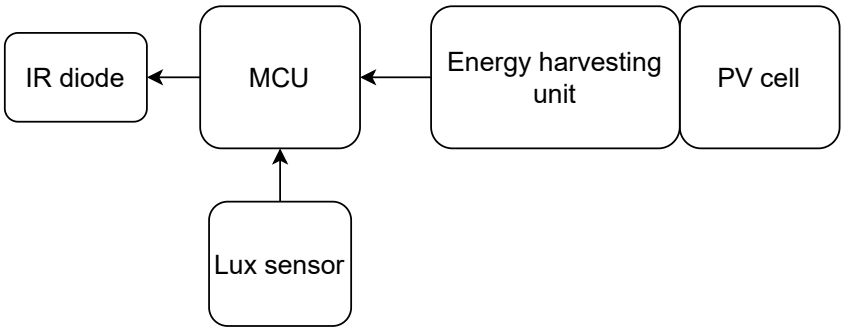

Figure 15. LIoT Node.

Printed Perovskite PV cell along with supercapacitors and energy harvesting unit with maximum power point tracking (MPPT) feature were designed to optimally power the MCU, Lux sensor and IR diode. The MCU and Lux sensor were optimised to consume as little energy as possible and the communication between them using I2C protocol was established. Sensor's readings are encapsulated into NEC protocol and transmitted by means of a off-the-shelf infrared diode.

4.1.1 Modulation

In the project, a popular NEC infrared protocol was used to encode transmitted bits. The protocol leverages pulse distance encoding where logical 0 comprises of 562.5 μs burst followed by a 562.5 μs space and logical 1 comprises of 562.5 μs burst followed by a 1.6875 ms space. Bits are carried on 38 kHz which is a typical carrier frequency used in infrared remote control devices to distinguish the signal from noise. Figure 16 illustrates the timing of bits.

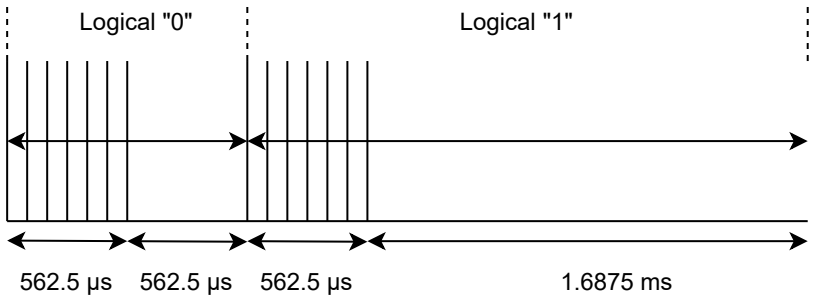

Figure 16. Bit representation used in NEC protocol.

NEC frame was depicted in Figure 17. The pulse begins with 9 ms AGC burst which originally used to set the gain of IR receivers followed by a space. Next, address and command are being transmitted with least significant bit (LSB) first. So as to be able to determine the value of the last bit one extra burst is needed at the end of the frame.

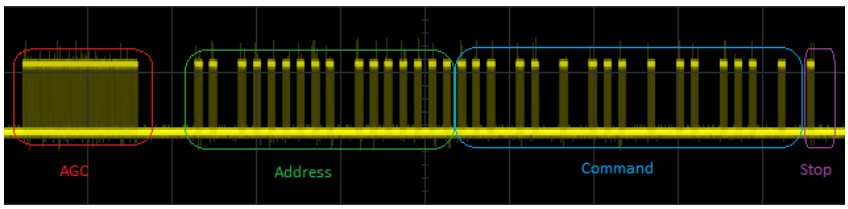

Figure 17. Typical NEC pulse train measured in the implemented LIoT node.

Both address and command fields can accommodate 16 bits each. However, there are two ways of allocating the bits. When reliability is prioritized, address and command, which now consist of 8 bits each, are transmitted twice. During the second transmission all bits are inverted which assists in verifying the correctness at the receiver. Also, the total transmission time is constant because each bit is flipped with its inverted length. Another way which reduces reliability is doing away with inverted bits and extending the address and command fields to 16 bits. In the project, the combination of these two approaches was implemented. Namely, address field is 8 bits and 8 inverted bits and command field is extended to 16 bits. Thus, the available address space equals 256 and the payload (command) is 16 bits.

4.1.2 Energy harvesting

Three separate units were combined in order to harvest solar energy: printed Perovskite PV cell reused from the downlink system, two supercapacitors and energy harvesting IC. Energy harvesting IC developed by Jasper Sikken and dubbed AEMSUCA presented in Figure 18 harvests solar energy into two supercapacitors [59]. The board's heart - AEM10941 developed by e-peas was specifically dedicated to manage energy from multi-cell solar panels, store it in rechargeable elements and provide power with two independent regulated outputs. AEMSUCA was chosen for the project due to the following characteristics:

- very low cold start up from 380 mV and 3 μW input power,
- MPPT every 5 secs set to 70%,
- solar input voltage from 50 mV to 5 V,
- two supercapacitors connected in series as a storage element,
- capacitors are charged up to 4.5 V,
- 3.3 V / 80 mA output compatible with Arduino Pro Mini.

AEMSUCA output enable and disable thresholds were given in Table 2.

Table 2. Enable and cut-off threshold for AEMSUCA.

Enable threshold	Disable threshold
3.92 V	3.6 V

Figure 18. AEMSUCA Solar Harvesting IC.

At any given point in time, solar cell operates at particular voltage and current which is known as an operating point. The position of the operating point depends on the temperature, irradiance and electrical load seen by the cell at its output. By using the formula

$$P = V \times I, \tag{20}$$

one can calculate power delivered to the load. Both I-V / P-V curves were presented in Figure 19.

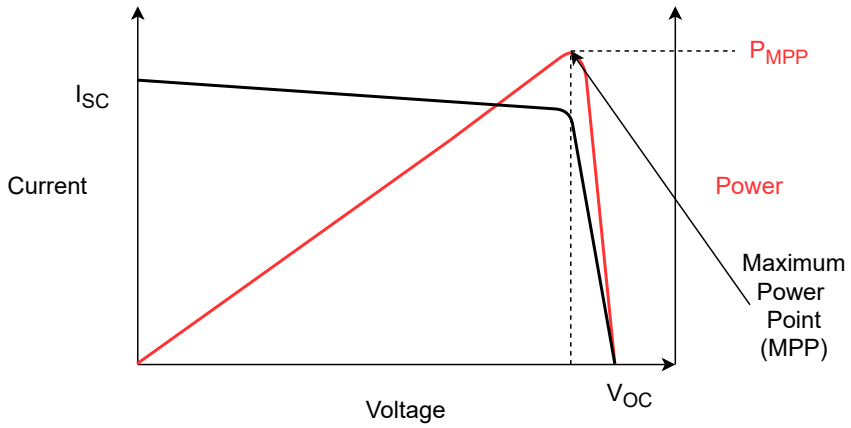

Figure 19. Generic I-V / P-V curve of a solar cell.

To get the maximum power delivered by the cell, it should operate at the maximum power point which is located at the peak of the power curve and is usually equivalent to between 50% to 80% of the open circuit voltage (V_{OC}). However, if ambient conditions fluctuate, so does the MPP. To steadily monitor the location of MPP tracking algorithms have been conceived such as Fractional Open Circuit Voltage or Perturb and Observe method, to name a few. MPPT can yield significant advantage when ambient conditions such as light intensity change over time.

Due to the fact that the solar cell can output more than 5 V which is the maximum voltage the AEMSUCA can handle, a voltage regulator was added. A Zener diode fits well to the application by limiting the voltage to 5 V. The I-V characteristic of a Zener diode is drawn in Figure 20. When in forward bias, the diode behaves as a regular diode by allowing the current flow once forward voltage is reached. However, when biased reversely, voltage is all but constant for a wide range range of current values. As a result, the Zener based voltage regulator requires the diode to be biased in a reverse manner. The excessive voltage is burnt and emitted by the diode in the form of heat. In this case, when input voltage is lower than Zener voltage no current flows through the diode and the output voltage remains unchanged. A 5.1 V / 0.5 W Zener diode was used in the implementation.

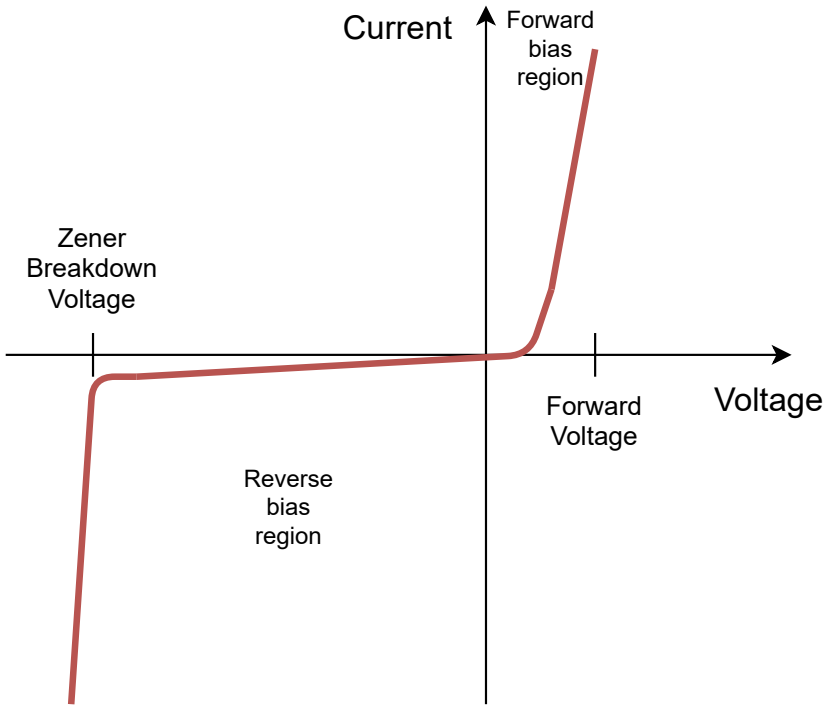

Figure 20. I-V characteristic of Zener diode.

The choice of capacitors is of fundamental importance since a trade-off between charging and discharging times has to be reached. The electrical charge stored in a capacitor can be expressed as

$$Q = C \times V, \tag{21}$$

where

C denotes nominal capacitance in Farads.

Because there are two capacitors connected in series the total capacitance C_T is given by

$$C_T = \frac{1}{\frac{1}{C_1} + \frac{1}{C_2}}, \tag{22}$$

where

C_1, C_2 are consecutive capacitors.

A ballpark estimation of the operating time of LIoT node can be obtained by the formula

$$T = C_T \times \frac{(V_C - V_{disable})}{I_{node}}, \tag{23}$$

where

V_C is voltage across capacitors with max value equal to 4.5 V,
$V_{disable}$ disable voltage threshold equal to 3.6 V,
I_{node} is current drawn by the node.

Since capacitance determines both the operating and charging time it is crucial to choose the adequate capacitors for the application's requirements. The LIoT node was tested with two pairs of electrolytic supercapacitors: 10 F 2.7 V AVX and 1.5 F 2.5 V Aerogel which boast low cost, low leakage current and reasonable dimensions. The complete picture of the energy harvesting unit is shown in Figure 21. The resistor R_s limits the current flowing through the diode but since current drawn from the AEMSUCA is not detrimental to the diode, the resistor was omitted.

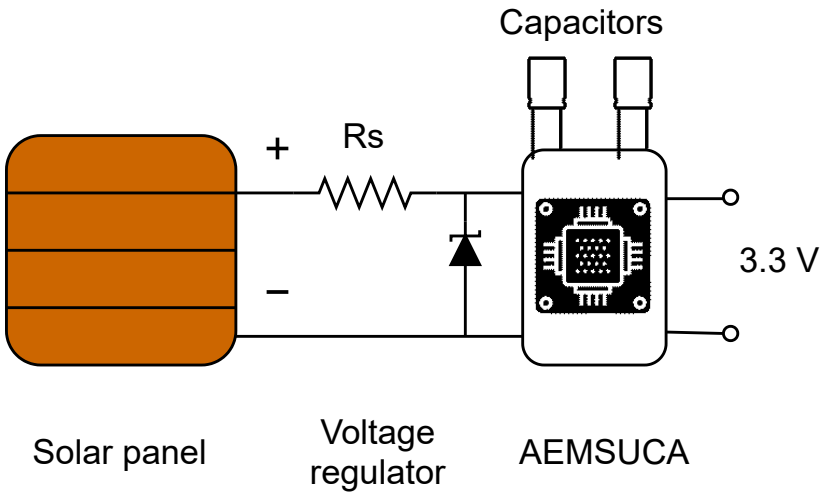

Figure 21. Energy harvesting diagram.

4.1.3 Lux sensor

In order to determine the ambient light intensity, the VEML7700 high accuracy ambient light sensor (ALS) created by Vishay Semiconductors and integrated into a breakout board by Adafruit Industries, was used. The complete product is shown in Figure 22. Except for the VEML7700, the board was equipped with a 3.3 V regulator and logic level shifter. The communication between the sensor and master device is established through universal the I2C protocol. The sensor's 16 bit dynamic range allows for ambient light detection varying from 0 lx to 120 klx, with resolution as low as 0.0036 lx/counts. In terms of power consumption, the sensor can be switched to shut down mode where the current is 0.5 μA and it also offers four power-saving modes (PSM). Before deployment, the sensor requires configuration which depends on lightning conditions and application requirements. Specifically, one should consider factors such as the light intensity operating range, resolution and frequency of measurement, and dynamics of light intensity change. By adjusting two parameters, gain and integration time, whose values are listed in Table 3, the sensor can be configured for the desired application.

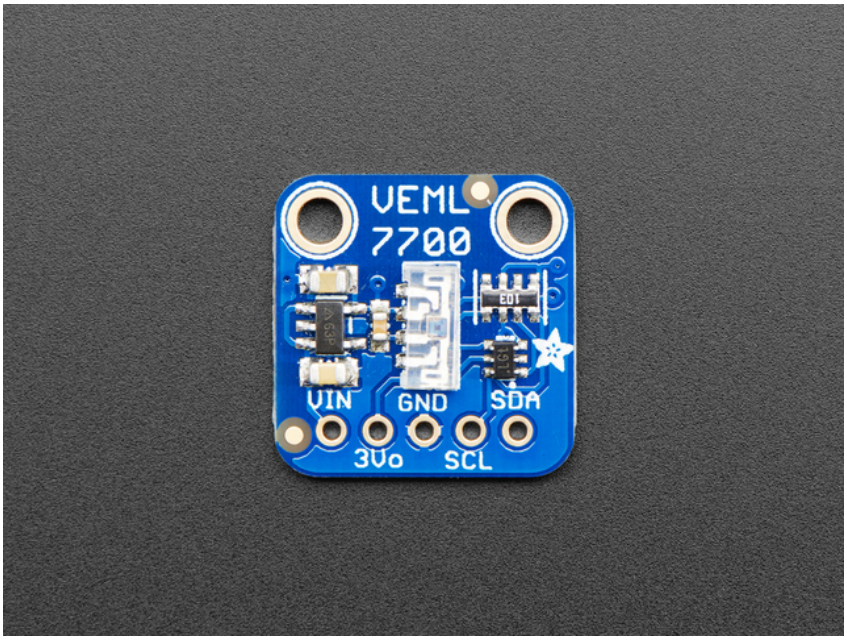

Figure 22. Adafruit VEML7700 ambient light sensor.

Table 3. Configuration values for VEML7700.

Gain	Integration time [ms]
1	25, 50, 100, 200, 400, 800
2	25, 50, 100, 200, 400, 800
1/8	25, 50, 100, 200, 400, 800
1/4	25, 50, 100, 200, 400, 800

Generally, higher gain is preferred in low light intensity conditions and higher integration time, which refers to the time during which the sensor holds the voltage signal as it maximizes and stabilizes resolution. The VEML7700 does also support four power-saving modes which reduce the drawn current at the cost of longer refresh time. Table 4 show how current and refresh time change for different PSMs when gain and integration time are constant.

Table 4. Gain, power-save mode, integration time, refresh time, I_{DD}, resolution.

Gain	PSM	Integration time (ms)	Refresh time (ms)	I_{DD} (μA)	Resolution (lx/bit)
2	1	100	600	8	0.0288
2	2	100	1100	5	0.0288
2	3	100	2100	3	0.0288
2	4	100	4100	2	0.0288

Since in the LIoT node the energy consumption must be prioritized and high resolution is not needed, the sensor was configured with gain equal to 2, integration time equal to 100 ms and the chosen PSM was 3, which gives the current drawn equal to 3 μA. The light intensity reading is kept in binary form in 16 bit ALS read-only register. In order to obtain the value in lux, one has to multiply the decimal value of ALS by the resolution typical for the chosen gain and integration time.

4.1.4 Transmitter's MCU

To combine the ease of implementation and the low-power consumption requirement Arduino Pro Mini with ATmega328P 3.3 V 8 MHz was picked to perform an I2C communication, encoding and modulation. The following adjustments have been made to minimize the current drawn by the Arduino:

- disabling ADC,
- turning off clock to serial peripheral interface (SPI),
- introduction of the deepest sleep possible for the MCU,
- introduction of watchdog timer to wake up the MCU.

The transmitter's algorithm was presented in Figure 23, which was based on code written in Arduino IDE. In a nutshell, the MCU goes into deep sleep, wakes up after watchdog timer goes off, reads and transmits the sensor's data and relapses into sleep.

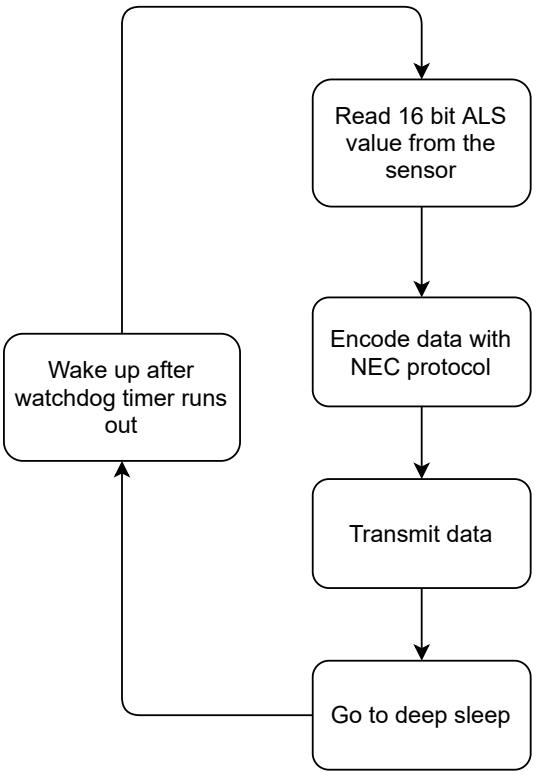

Figure 23. Transmitter algorithm.

The schematic of the LIoT node is presented in Figure 38.

4.2 Access Point - Receiver

The task of the access point is to detect, demodulate and decode infrared signals coming from LIoT node. The access point consists of the MCU and photodiode-based receiver. The schematic of the AP is presented in Figure 37.

4.2.1 IR photodiode based reception

In order to receive the signal VMA317 infrared receiver was used in implementation. It comprises of photodiode and preamplifier compactly packed in one module. The choice of the receiver was based on the following characteristics:

- TTL levels compatibility,
- supply voltage 3 - 5 VDC,
- shield against electric field disturbance and interferences,
- high immunity against ambient light,
- band pass filter at center frequency 37.9 kHz,
- Arduino compatible and commercially available.

The IR receiver performs two fundamental steps. First, the noise is filtered out at the frequency of around 38 kHz so that the transmitted signal can be distinguished from other possible infrared sources present in the environment. Next, it is demodulated by removing the carrier frequency and determining the bit values which are presented in Figure 24.

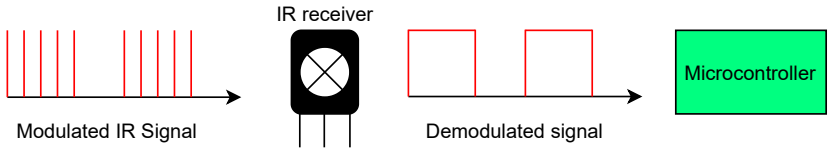

Figure 24. PD-based receiver demodulation.

4.2.2 Receiver's MCU

Since the access point is not constrained by power, the Arduino Uno ATmega328P 16MHz was picked as the MCU. The receiver's algorithm is shown in Figure 25.

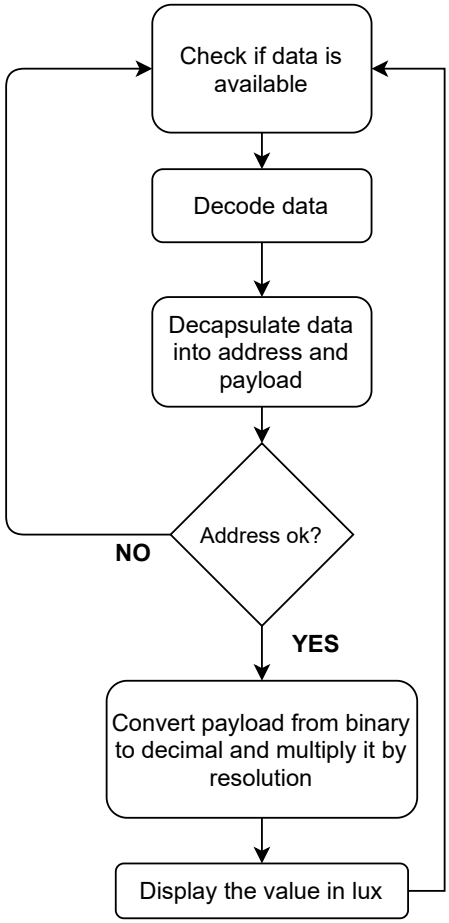

Figure 25. Receiver algorithm.

The ready prototype is shown in Figure 26.

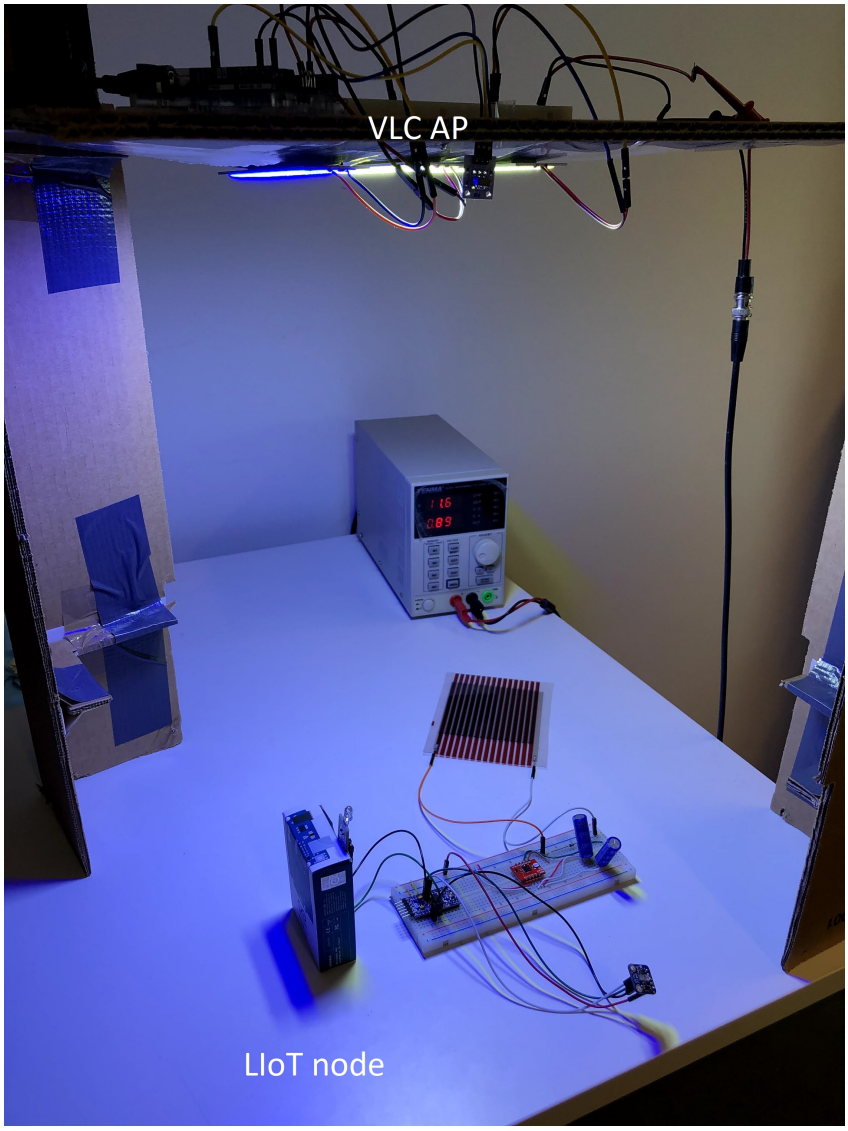

Figure 26. VLC uplink testbed.

5 PERFORMANCE EVALUATION

5.1 Transmitted and received frames

The transmitted and received frames are depicted in Figure 27. It can be observed that the transmitted frame contains the carrier and the received one shows an already demodulated signal. The bottom frame is inverted because the PD-based receiver holds the voltage high when not receiving any signal.

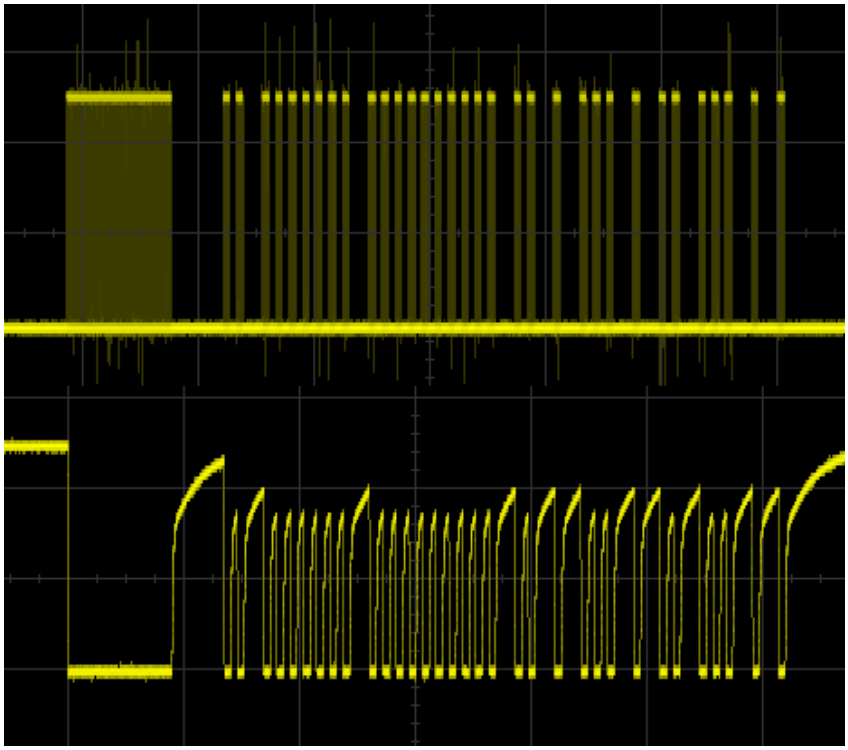

Figure 27. Transmitted (upper) and received (bottom) NEC frames.

5.2 BER measurement

BER can be calculated by the formula

$$BER = \frac{N_{error}}{N_{total}}, \tag{24}$$

where

N_{error} is the number of erroneous bits,
N_{total} is the number of transmitted bits in total.

BER measurement campaign was performed for three scenarios listed below:

- Scenario 1: LIoT node stationary, LOS - Figure 28,

- Scenario 2: LIoT node moving, LOS - Figure 30,
- Scenario 3: NLOS - Figure 32.

The BER algorithm presented in Figure 39 was implemented in Matlab. At every distance step the access point waits until 1000 frames are received, which amounts to 32000 bits. Next, the received bits are compared by XOR operation with the original sequence so as to calculate BER. Two additional characters were added at the end of every transmitted frame that is carrier return and linefeed, in order to distinguish separate frames. Since the algorithm compares the received frame with the original frame one by one, the 100 ms interval was added between transmitted frames so that receiver could keep up with processing. Times shorter than 100 ms resulted in extraordinary high BER due to receiver's inability to receive, decode and process the data within this period.

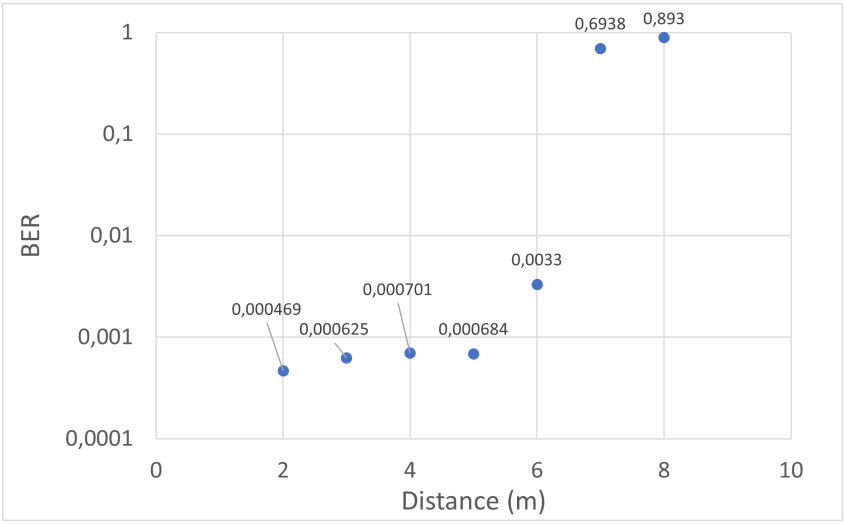

Figure 28. BER vs distance - Scenario 1.

In case LIoT node remained stationary and LOS condition was met, BER deteriorated considerably only as soon as the distance reached 7 m. Figure 29 shows the LOS alignment between transmitter and receiver.

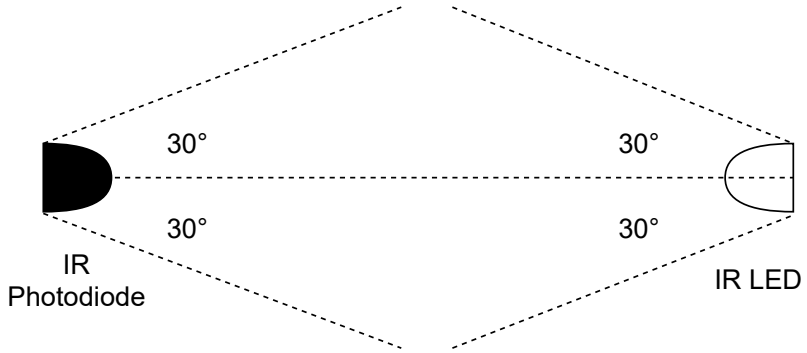

Figure 29. Photodiode - LED alignment.

It was observed that correct reception was not possible if transmitter's or receiver's angles were over 30°. Scenario 2 saw a slight increase in BER, chiefly on account of LIoT node movement during which photodiode and LED were not always aligned within the angle.

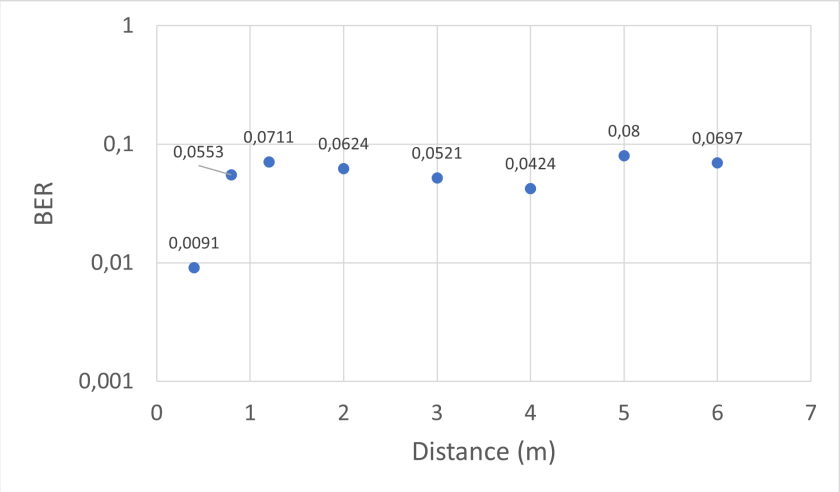

Figure 30. BER vs distance - Scenario 2.

Due to the fact that direct alignment is required to establish a one-way communication, the following setup depicted in Figure 31 was made in order to measure BER in NLOS scenario.

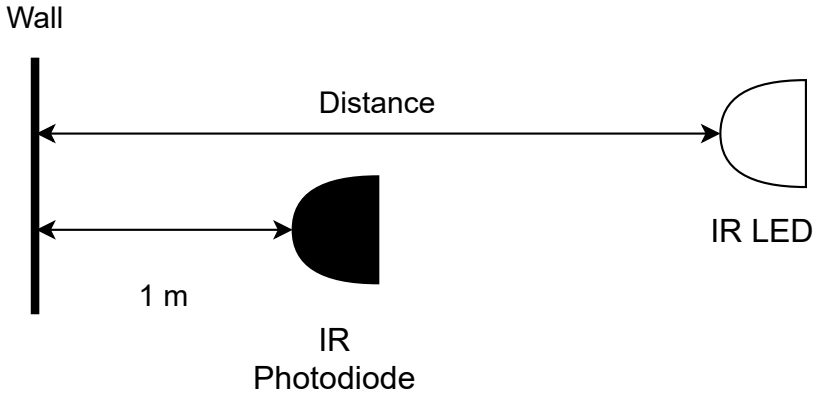

Figure 31. Scenario 3 NLOS alignment.

The system proved to reach satisfactory BER (Figure 32) even when the signal was reflected from the wall. Similarly to previous scenarios BER soared dramatically when total distance reached around 7 m.

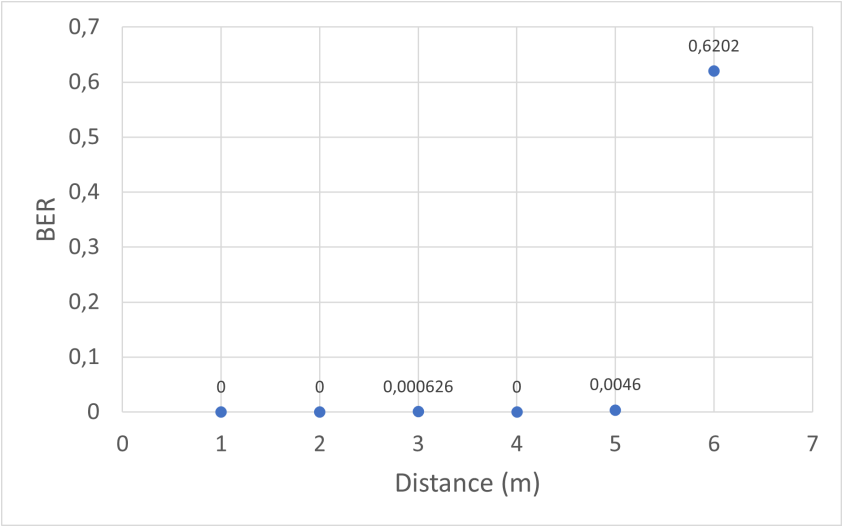

Figure 32. BER vs distance - Scenario 3.

The aforementioned results suggest that IR uplink can be successfully deployed to transmit sensor's data up to certain range.

5.3 Received SNR measurement

SNR at the receiver was measured according to formula

$$SNR = 20 \log_{10}(\frac{V_{signal}}{V_{noise}}), \tag{25}$$

where

V_{signal} is signal voltage,
V_{noise} is noise floor level.

The measurements were conducted by inspecting the voltages at the output of infrared L53P3BT photodiode. Figure 33 shows declining SNR as distance increases. At the distance of around 9 m it was impossible to measure SNR by reading from oscilloscope because the signal became masked by the noise.

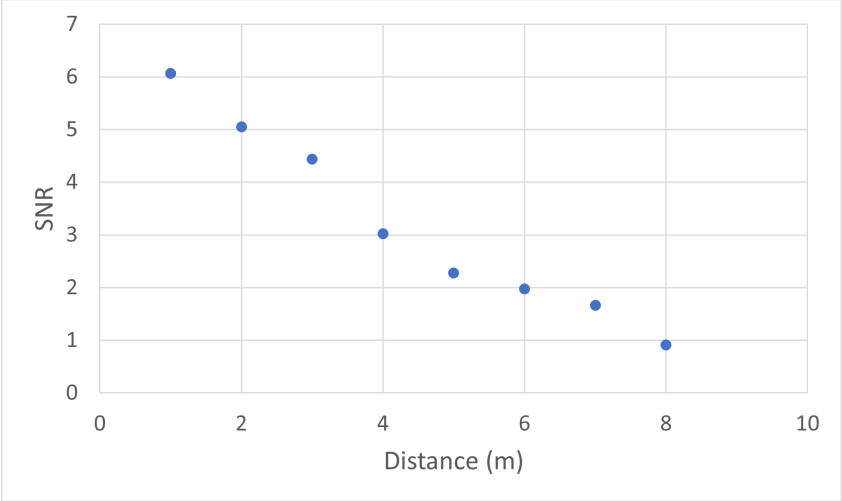

Figure 33. Received SNR vs distance.

Nevertheless, the link distance for which receiver module was able to correctly receive and decode data was measured to be between 6 - 8 m. This fact emphasises the role of filtration and amplification at the receiver even in the presence of low SNR.

5.4 Energy harvesting performance

The LIoT node current consumption at 3.3 V is shown in Table 5. The read and send burst refers to the period when MCU wakes up and falls sleep and it was measured between 40 to 80 mA and the average is given. The values in Table 5 were obtained by multimeter.

Table 5. LIoT node power consumption.

Deep sleep	Read and Send burst
20 μA	60 mA

5.4.1 Cold start behaviour

Cold start charging efficiency of the AEMSUCA was tested with two pairs of capacitors: 0.022 F 5.5 V and 1.5 F 2.5 V. All the results were produced in indoor lightning of 600 lux. By observing the rising voltage across capacitors from 0 V up to output-enabling voltage it is possible to estimate the charging power

$$P_{charge} = \frac{Q}{t}, \tag{26}$$

where

Q denotes electrical charge given in (21),

t is the elapsed time.

To evaluate the proper functioning of the AEMSUCA, relatively small 0.022 F capacitors were used to capture the charging characteristic in one picture. In Figure 34, the upper green line represents voltage across capacitors and the bottom yellow line represents the solar cell input voltage. It can be deducted that capacitors were charged up to 4.5 V (2 V/div) in around 300 s (50 s/div) which gives an estimate charging power equal to 0.165 mW. The capacitors were able to charge to the maximum value because during this test there was no current drawn from the energy harvesting unit.

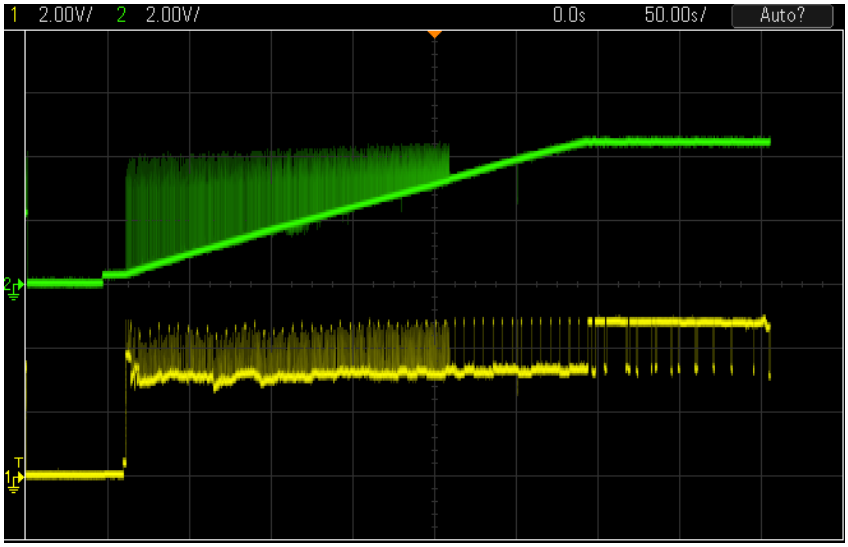

Figure 34. Cold start charging $C_T = 0.011$ F up to 4.5 V.

The cold start was also tested with 1.5 F capacitors. Figure 35 shows the initial phase of charging with voltage across capacitors equal to zero and input solar cell voltage equal to 3.6 V. One can also observe regular voltage peaks in solar panel output (yellow) which corresponds to MPPT every 5 secs.

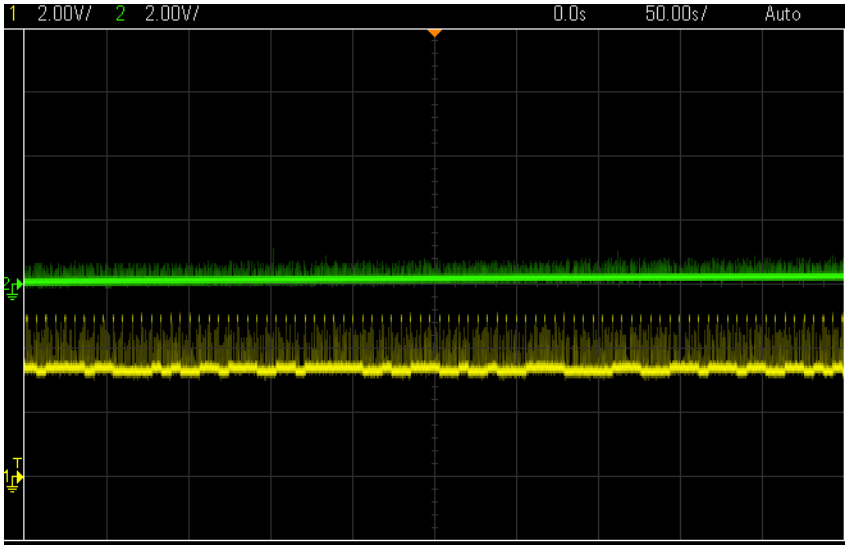

Figure 35. Cold start charging $C_T = 0.75$ F - beginning.

After exactly 4 h 9 mins of charging, the capacitors reached the enable threshold which is shown in Figure 36. Thus the charging power equals 0.197 mW.

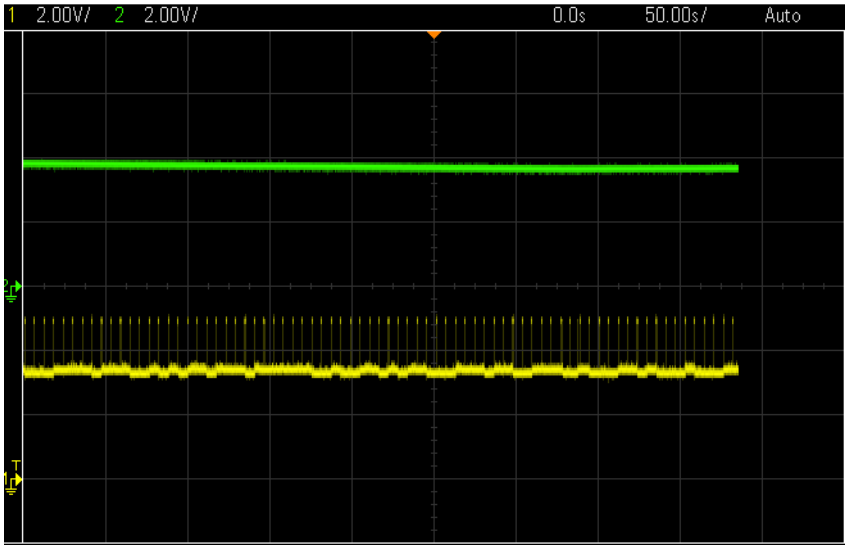

Figure 36. Cold start charging $C_T = 0.75$ F up to 3.92 V - Enable threshold achieved.

5.4.2 Normal behaviour

Charging and operating times, charging power and application's estimated current consumption were measured for 1.5 F and 10 F capacitors resulting in total capacitance equal to 0.75 F and 5 F, respectively. Measurements shown in Table 6 were obtained in normal mode when capacitors were already charged to the enable threshold voltage. Charging time is the time that elapsed between capacitors charging from disable to enable thresholds and operating time is the time when capacitors discharge from enable

to disable voltages. Charging power was estimated by manipulating (26) and node's current consumption according to (23).

Table 6. Comparison between two total capacitances.

	$C_T = 0.75$ F	$C_T = 5$ F
T_{charge} [mins]	20	122
$T_{operate}$ [mins]	8	37
P_{cold} [mW]	0.197	-
P_{normal} [mW]	0.206	0.218
I_{app} [mA]	0.51	0.7

6 DISCUSSION

The design, implementation and evaluation of a LIoT node were described in the thesis. The main objective of this thesis was to establish an uplink connection while harvesting energy needed to power the electronics from ambient light. Since the type and size of data to be transmitted vary depending on application, it was decided that the LIoT node would send a 32 bit long data packet at regular intervals of 4 sec. Consequently, as energy was at a premium, the design required reducing the energy consumption as much as possible. As indicated in the literature review infrared light can be successfully integrated into the system as a robust carrier. While it enjoys numerous advantages such as supporting relatively long distance, commercial availability of inexpensive electronics and straightforward implementation, the IR LEDs consume the best part of available energy and may not be suitable for ultra low power applications. In addition, it may cause interferences with already existing IR devices such as TV remotes. One solution to decrease the consumption of traditional IR LED would be to use a printed one. Unfortunately, their performance leaves a lot to be desired and the current state of printed IR LEDs is not satisfactory for even prototyping. The developed LIoT node was calculated to consume around 600 μA at 3.3 V whereas the most advanced retroreflector based transmitting circuit (ViTag described in Section 3.2) was measured to consume 36.69 μA at 2.6 V. Additionally, with the current progress in manufacturing better and better printed electrochromic displays it may be possible to bring these numbers down by substituting power-hungry LCDs with ultra low energy printed electrochromic displays as modulators. Thus, infrared light is not the most suitable uplink approach from the energy efficiency standpoint. With so many modulation techniques theoretically developed and optimised for VLC, the most widespread consumer protocols used in IR rely predominantly on PPM. A popular NEC protocol with error detection capability served the purpose by successfully allocating 16-bit long sensor reading into the payload. One protocol enhancement would entail shortening the address field at the cost of lengthening payload field. Eight-bit long address used in the implementation seems to be too long as 256 access points are unlikely to be in the vicinity of the LIoT node. The compact design of the node was achieved by resorting to only one printed Perovskite solar cell and two supercapacitors. Unfortunately, as reported in [10], these cells perform poorly under warm white ($<$ 4500K). It should be emphasised that if conventional solar cell was used in the design it would have produced significantly more energy as opposed to the printed cell. However, mixed cool white and warm lightning together with novel energy harvesting unit AEMSUCA made it possible to efficiently deliver power within reasonable time frame. Additionally, MPPT helps to deliver optimal power with changing lightning conditions. The capacitors' nominal capacitance determines the charging and operating time. By choosing the capacitance small enough to sustain the LIoT node only for transmitting one packet at a time the concept "Expose and Connect" could be realized. In the implementation, three capacitance values were used. The lowest one, 0.022 F, was not enough to allow for one transmission. However, by inspecting the oscilloscope it was predicted that value slightly higher such as 0.05 F would potentially be well enough for just transmitting one packet. The performance of energy harvesting unit was tested with other two supercapacitors of much higher capacitances, as shown in Table 6. Two components of the LIoT node, MCU and lux sensor, were programmed to decrease the drawn current. Introduction of deep sleep, disabling all unused features in

power reduction registers as well as low power configuration of the lux sensor contributed to reducing the current drawn during idle state from 12 mA to 20 μA. Most of the focus and work were placed on the LIoT node and, as a result, access point performs simple reception of infrared signal. By using ready, off-the-shelf components the uplink connection was established along with solar energy harvesting. Such prototype could be used in indoor environment to regularly provide feedback or sensor's readings. Because the link is vulnerable to blockage and misalignment between transmitter and receiver beam steering and omnidirectional optical antennas could be incorporated to ensure connectivity between nonstationary LIoT node and access point.

7 CONCLUSION AND FUTURE WORK

In the thesis, fundamentals of VLC were introduced followed by a description of prospective uplink solutions. Throughout the literature review it was concluded that infrared should be investigated first as the most viable and straightforward solution. First, the communication between LIoT node and AP was established by sending arbitrary data by means of the NEC protocol. Next, lux sensor was included in the design with real data being embedded into the protocol. Once this step was complete, MCU and lux sensor were optimised for lowest energy consumption by various techniques. Last but not least, solar cell, supercapacitors and energy harvesting unit were incorporated into the design. In the end, the system was tested with BER and SNR measurements as well as energy harvesting performance was analyzed. Altogether, the system lived up to the requirements set in the initial state of thesis work.

Further work may be focused on either providing two-way communication by combining uplink with downlink or improving the uplink towards lesser power consumption. As regards the former choice, the challenge arises when it comes to providing sufficient power for both receiving and transmitting parts and, preferably, displaying information and reading sensors' data. It may be worthwhile to substitute the current AEMSUCA and elecrotolytic supercapacitors with AEMLIC and lithium ion capacitors. The AEMLIC, with the same e-peas chip, converts solar panel energy into lithium ion capacitors which boast very high energy density in comparison to traditional supercapacitors. For instance, 100 F 3.8 V lithium ion capacitor can be used in the project. AEMLIC is capable of outputting only 2.2 V so voltage booster would be necessary to implement to power Arduino Pro Mini. Alternatively, at some point, Pro Mini is to be replaced with dedicated system on chip (SoC) which can use for instance MSP430 microcontrollers by Texas Instruments, for instance. In order to minimize the LIoT node power consumption, one should do away with LED transmission and switch to passive uplink which would not require active transmission and which was proved to yield significant energy savings. Also, moving towards fully-printed LIoT node is desired, however it is constrained by the advancements in PE technology. Another approach would consists in replacing traditional LEDs with printed ones. Although they are still in their infancy they consume less power and are envisioned to be used within Living Surfaces concept. On the other hand, ultra sensitive and directional receivers had to be used to receive data modulated using these printed LEDs because of their low illuminance. Whereas VLC poses a multitude of engineering challenges, it is an exciting area to delve into because of its inherent assumptions and the opportunity to give shape to the interconnected world from scratch.

8 REFERENCES

[1] (2017) 5G Systems, Enabling the transformation of industry and society. Ericsson, p. 5.

[2] CISCO (2019) Cisco Visual Networking Index: Global Mobile Data Traffic Forecast Update, 2017–2022 , pp. 15–16.

[3] Mahmood N.H., López O. & Park O.S. (2020) White paper on critical and massive machine type communication towards 6G. 6G Research visions, University of Oulu , p. 8.

[4] Cogalan T. & Haas H. (2017) Why would 5g need optical wireless communications? In: 2017 IEEE 28th Annual International Symposium on Personal, Indoor, and Mobile Radio Communications (PIMRC), pp. 1–6.

[5] Arfaoui M.A., Soltani M.D., Tavakkolnia I., Ghrayeb A., Assi C., Safari M. & Haas H. (2020) Measurements-based channel models for indoor lifi systems. IEEE Transactions on Wireless Communications , p. 1.

[6] Haas H. (2019) Opportunities and challenges of future lifi. In: 2019 IEEE Photonics Conference (IPC), p. 2.

[7] Islim M.S., Ferreira R.X., He X., Xie E., Videv S., Viola S., Watson S., Bamiedakis N., Penty R.V., White I.H., Kelly A.E., Gu E., Haas H. & Dawson M.D. (2017) Towards 10 Gb/s orthogonal frequency division multiplexing-based visible light communication using a gan violet micro-led. Photon. Res. 5, pp. A35–A43. URL: http://www.osapublishing.org/prj/abstract.cfm?URI=prj-5-2-A35.

[8] Lin B., Tang X., Ghassemlooy Z., Lin C., Zhang M., Zhou Z., Wu Y. & Li H. (2017) A noma scheme for visible light communications using a single carrier transmission. In: 2017 First South American Colloquium on Visible Light Communications (SACVLC), p. 2.

[9] Burchardt H., Serafimovski N., Tsonev D., Videv S. & Haas H. (2014) Vlc: Beyond point-to-point communication. IEEE Communications Magazine 52, pp. 98–105.

[10] Perera M.A.N. (2020) Design and implementation of a light-based IoT (LIoT) node using printed electronics. Master's thesis, University of Oulu.

[11] Hamza M., Rehman M.U., Riaz A., Maqsood Z. & Khan W.T. (2021) Hybrid dual band radio frequency and solar energy harvesting system for making battery-less sensing nodes. In: 2021 IEEE Radio and Wireless Symposium (RWS), pp. 116–118.

[12] Chang J., Ge T. & Sanchez-Sinencio E. (2012) Challenges of printed electronics on flexible substrates. In: 2012 IEEE 55th International Midwest Symposium on Circuits and Systems (MWSCAS), pp. 582–585.

[13] Haas H. (2018) Lifi is a paradigm-shifting 5g technology. Reviews in Physics , p. 1.

[14] (2019) IEEE standard for local and metropolitan area networks–part 15.7: Short-range optical wireless communications. IEEE Std 802.15.7-2018 (Revision of IEEE Std 802.15.7-2011) , pp. 1–407.

[15] Jackson D.K., Buffaloe T.K. & Leeb S.B. (1998) Fiat lux: a fluorescent lamp digital transceiver. IEEE Transactions on Industry Applications 34, pp. 625–630.

[16] Pang G., Kwan T., Chi-Ho Chan & Hugh Liu (1999) Led traffic light as a communications device. In: Proceedings 199 IEEE/IEEJ/JSAI International Conference on Intelligent Transportation Systems (Cat. No.99TH8383), pp. 788–793.

[17] Tanaka Y., Haruyama S. & Nakagawa M. (2000) Wireless optical transmissions with white colored led for wireless home links. In: 11th IEEE International Symposium on Personal Indoor and Mobile Radio Communications. PIMRC 2000. Proceedings (Cat. No.00TH8525), vol. 2, vol. 2, pp. 1325–1329 vol.2.

[18] Zhaocheng W., Qi W., Huang W. & Zhengyuan X. (2017) Visible light communications Modulation and Signal Processing. Wiley.

[19] Tsonev D., Videv S. & Haas H. (2013) Light fidelity (li-fi): Towards all-optical networking. vol. 9007, p. 900702.

[20] Brandl P., Enne R., Jukić T. & Zimmermann H. (2015) Owc using a fully integrated optical receiver with large-diameter apd. IEEE Photonics Technology Letters 27, pp. 482–485.

[21] Milovančev D., Jukić T., Vokić N., Brandl P., Steindl B. & Zimmermann H. (2021) Vlc using 800-μm diameter apd receiver integrated in standard 0.35-μm bicmos technology. IEEE Photonics Journal 13, pp. 1–13.

[22] Pathak P.H., Feng X., Hu P. & Mohapatra P. (2015) Visible light communication, networking, and sensing: A survey, potential and challenges. IEEE Communications Surveys Tutorials 17, pp. 2047–2077.

[23] Fuada S., Putra A.P., Aska Y. & Adiono T. (2016) Trans-impedance amplifier (ha) design for visible light communication (vlc) using commercially available op-amp. In: 2016 3rd International Conference on Information Technology, Computer, and Electrical Engineering (ICITACEE), pp. 31–36.

[24] Xiao Q., Ge G. & Wang J. (2009) The neural network adaptive filter model based on wavelet transform. In: 2009 Ninth International Conference on Hybrid Intelligent Systems, vol. 1, vol. 1, pp. 529–534.

[25] Nazari Golpayegani G. & Jafari A. (2009) Improved adaptive neural fuzzy filter and its application in noise cancellation. In: 2009 3rd International Conference on Bioinformatics and Biomedical Engineering, pp. 1–7.

[26] He W., Zhang M., Wang X., Zhou H. & Ren X. (2019) Design and implementation of adaptive filtering algorithm for vlc based on convolutional neural network. In: 2019 IEEE 5th International Conference on Computer and Communications (ICCC), pp. 317–321.

[27] (accessed 02.02.2021.), Understanding and eliminating 1/f noise. URL: https://www.analog.com/en/analog-dialogue/articles/understanding-and-eliminating-1-f-noise.html#.

[28] Hussain B., Li X., Che F., Patrick Yue C. & Wu L. (2015) Visible light communication system design and link budget analysis. Journal of Lightwave Technology 33, pp. 5201–5209.

[29] Ahmed F., Ali S. & Jawaid M. (2018) A review of modulation schemes for visible light communication. INTERNATIONAL JOURNAL OF COMPUTER SCIENCE AND NETWORK SECURITY 18, pp. 117–125.

[30] Aliaberi A., Sofotasios P.C. & Muhaidat S. (2019) Modulation schemes for visible light communications. In: 2019 International Conference on Advanced Communication Technologies and Networking (CommNet), pp. 1–10.

[31] Manimegalai C.T., Gauni S., Raghavan N. & Rao T.R. (2017) Investigations on suitable modulation techniques for visible light communications. In: 2017 International Conference on Wireless Communications, Signal Processing and Networking (WiSPNET), pp. 1818–1822.

[32] Akande K.O., Haigh P.A. & Popoola W.O. (2018) On the implementation of carrierless amplitude and phase modulation in visible light communication. IEEE Access 6, pp. 60532–60546.

[33] 3GPP (2009) Evolved universal terrestrial radio access (e-utra). Technical Specification (TS) 36.211, 3rd Generation Partnership Project (3GPP). Version 8.9.0.

[34] Tsonev D., Videv S. & Haas H. (2015) Unlocking spectral efficiency in intensity modulation and direct detection systems. IEEE Journal on Selected Areas in Communications 33, pp. 1758–1770.

[35] Gunawan W.H., Liu Y., Yeh C.H. & Chow C.W. (2020) Color-shift-keying embedded direct-current optical-orthogonal-frequency-division-multiplexing (csk-dco-ofdm) for visible light communications (vlc). IEEE Photonics Journal 12, pp. 1–5.

[36] Katz M. & O'Brien D. (2019) Exploiting novel concepts for visible light communications: from light-based IoT to living surfaces. Optik , pp. 214–232.

[37] Pérez-Nicoli P., Silveira F., Zhang X. & Amara A. (2016) Uplink wireless transmission overview in bi-directional vlc systems. In: 2016 IEEE International Conference on Electronics, Circuits and Systems (ICECS), pp. 588–591.

[38] Koumaras H., Makris D., Foteas A., Xilouris G., Kourtis M., Koumaras V. & Cosmas J. (2018) A sdn-based wifi-vlc coupled system for optimised service provision in 5g networks. In: 2018 IEEE 19th International Symposium on "A World of Wireless, Mobile and Multimedia Networks" (WoWMoM), pp. 14–17.

[39] Alenezi A.M. & Hamdi K.A. (2020) Reinforcement learning approach for hybrid wifi-vlc networks. In: 2020 IEEE 91st Vehicular Technology Conference (VTC2020-Spring), pp. 1–5.

[40] Gawłowicz P., Jarchlo E.A. & Zubow A. (2020) Bringing mimo to vlc using cots wifi. In: 2020 IEEE International Conference on Communications Workshops (ICC Workshops), pp. 1–6.

[41] Yang L., Zhang Q., Zhang W., Deng L. & Yang H. (2020) Resource allocation for hybrid visible light communications (vlc)-wifi networks. IEEE Access 8, pp. 176588–176597.

[42] Cossu G., Corsini R. & Ciaramella E. (2014) High-speed bi-directional optical wireless system in non-directed line-of-sight configuration. Journal of Lightwave Technology 32, pp. 2035–2040.

[43] Bui T. & Kiravittaya S. (2016) Demonstration of using camera communication based infrared led for uplink in indoor visible light communication. In: 2016 IEEE Sixth International Conference on Communications and Electronics (ICCE), pp. 71–76.

[44] Edirisinghe E.S.S., Karunarathna P.H.R.S.S., Dissanayake D.M.T.B. & Godaliyadda G.M.R.I. (2015) Design and implementation of a bi-directional visible light communication system. In: 2015 IEEE 10th International Conference on Industrial and Information Systems (ICIIS), pp. 519–524.

[45] Alsulami O.Z., Alresheedi M.T. & Elmirghani J.M.H. (2019) Infrared uplink design for visible light communication (vlc) systems with beam steering. In: 2019 IEEE International Conference on Computational Science and Engineering (CSE) and IEEE International Conference on Embedded and Ubiquitous Computing (EUC), pp. 57–60.

[46] Chen C., Basnayaka D.A., Purwita A.A., Wu X. & Haas H. (2020) Wireless infrared-based lifi uplink transmission with link blockage and random device orientation. IEEE Transactions on Communications , pp. 1–1.

[47] (accessed 08.02.2021.), Hollow retroreflector mirrors. URL: `https://www.thorlabs.com/newgrouppage9.cfm?objectgroup_id=12625`.

[48] Janik L., Novak M., Dobesch A. & Hudcova L. (2017) Retroreflective optical communication. In: 2017 Conference on Microwave Techniques (COMITE), pp. 1–4.

[49] Shao S., Khreishah A. & Khalil I. (2018) Retro: Retroreflector based visible light indoor localization for real-time tracking of iot devices. In: IEEE INFOCOM 2018 - IEEE Conference on Computer Communications, pp. 1025–1033.

[50] Shao S., Khreishah A. & Elgala H. (2017) Pixelated vlc-backscattering for self-charging indoor iot devices. IEEE Photonics Technology Letters 29, pp. 177–180.

[51] Li J., Liu A., Shen G., Li L., Sun C. & Zhao F. (2015) Retro-vlc: Enabling battery-free duplex visible light communication for mobile and iot applications. In: Proceedings of the 16th International Workshop on Mobile Computing Systems and Applications, HotMobile '15, Association for Computing Machinery, New York, NY, USA, p. 21–26. URL: `https://doi.org/10.1145/2699343.2699354`.

[52] Xu X., Shen Y., Yang J., Xu C., Shen G., Chen G. & Ni Y. (2017) Passivevlc: Enabling practical visible light backscatter communication for battery-free iot applications. In: Proceedings of the 23rd Annual International Conference on Mobile Computing and Networking, MobiCom '17, Association for Computing Machinery, New York, NY, USA, p. 180–192. URL: https://doi.org/10.1145/3117811.3117843.

[53] Müller H., Colley A., Häkkilä J., Jensen W. & Löchtefeld M. (2019) Using electrochromic displays to display ambient information and notifications. In: Adjunct Proceedings of the 2019 ACM International Joint Conference on Pervasive and Ubiquitous Computing and Proceedings of the 2019 ACM International Symposium on Wearable Computers, UbiComp/ISWC '19 Adjunct, Association for Computing Machinery, New York, NY, USA, p. 1075–1078. URL: https://doi.org/10.1145/3341162.3344844.

[54] (accessed 09.02.2021.), What is mems technology? URL: https://www.mems-exchange.org/MEMS/what-is.html.

[55] (accessed 09.02.2021.), Secure optical communication system utilizing deformable mems mirrors. URL: https://www.plxinc.com/white-papers/secure-optical-communication-system-utilizing-deformable-mems-mirrors.

[56] Sayyah K., Narayanan A., Persechini D. & Brewer P. (2005) Conformal pixellated mqw modulator structure for modulating retroreflector applications. IEEE Photonics Technology Letters 17, pp. 1854–1856.

[57] Cp J. & Jeyachitra r. (2020) Energy efficient bi-directional visible light communication using thin-film corner cube retroreflector for self-sustainable iot. IET Optoelectronics 14.

[58] (accessed 10.02.2021.), Endmemo. URL: http://www.endmemo.com/sconvert/luxwatt_squarecentimeter.php.

[59] (accessed 06.04.2021.), Solar harvesting into supercapacitors. URL: https://hackaday.io/project/160470-solar-harvesting-into-supercapacitors.

9 APPENDICES

Appendix 1 Receiver schematics

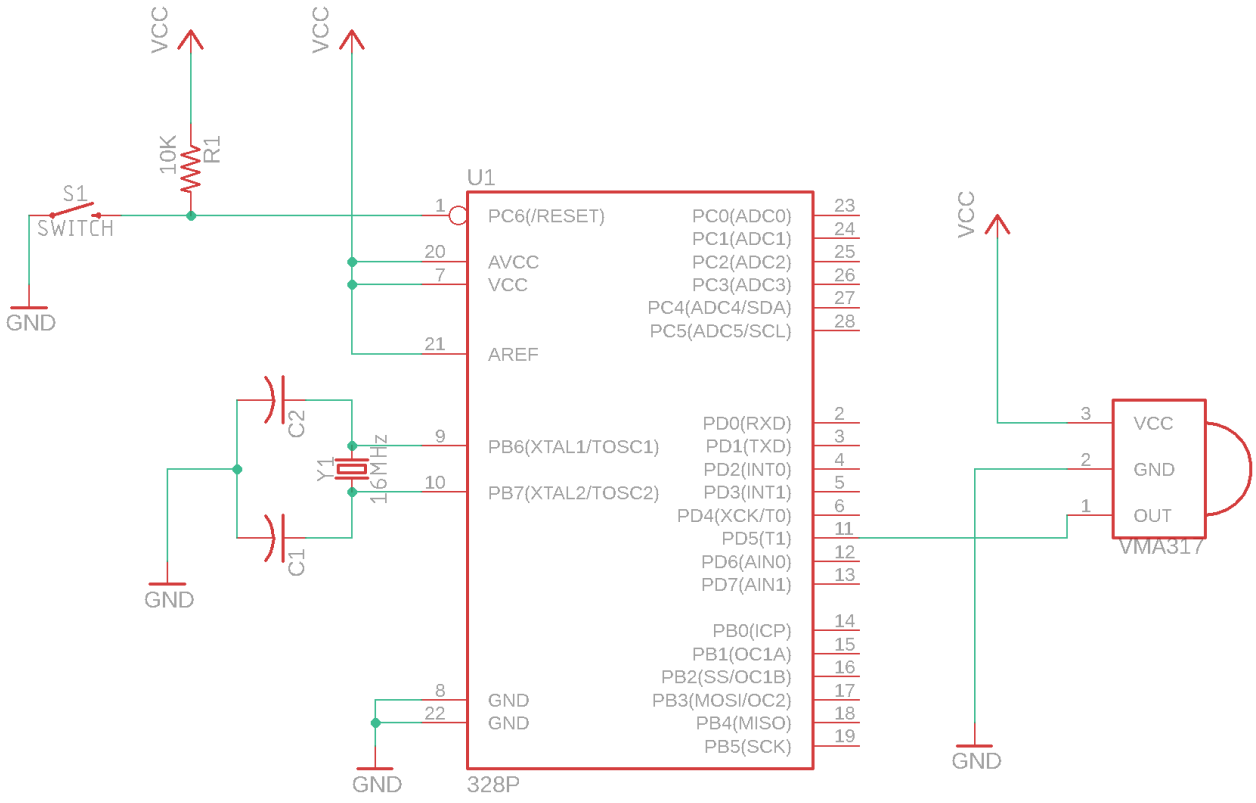

Figure 37. Access point schematics.

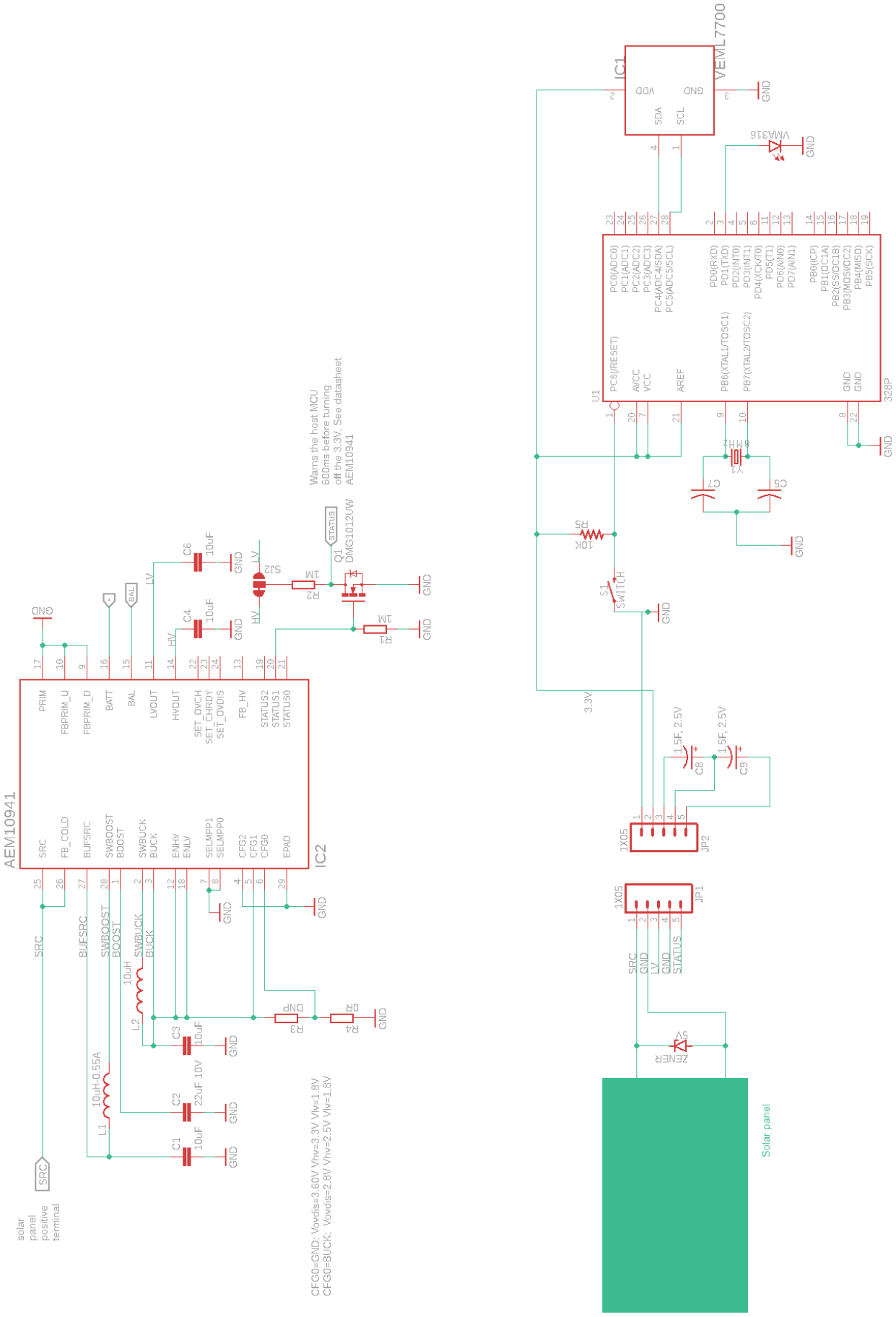

Figure 38. LIoT node schematics.

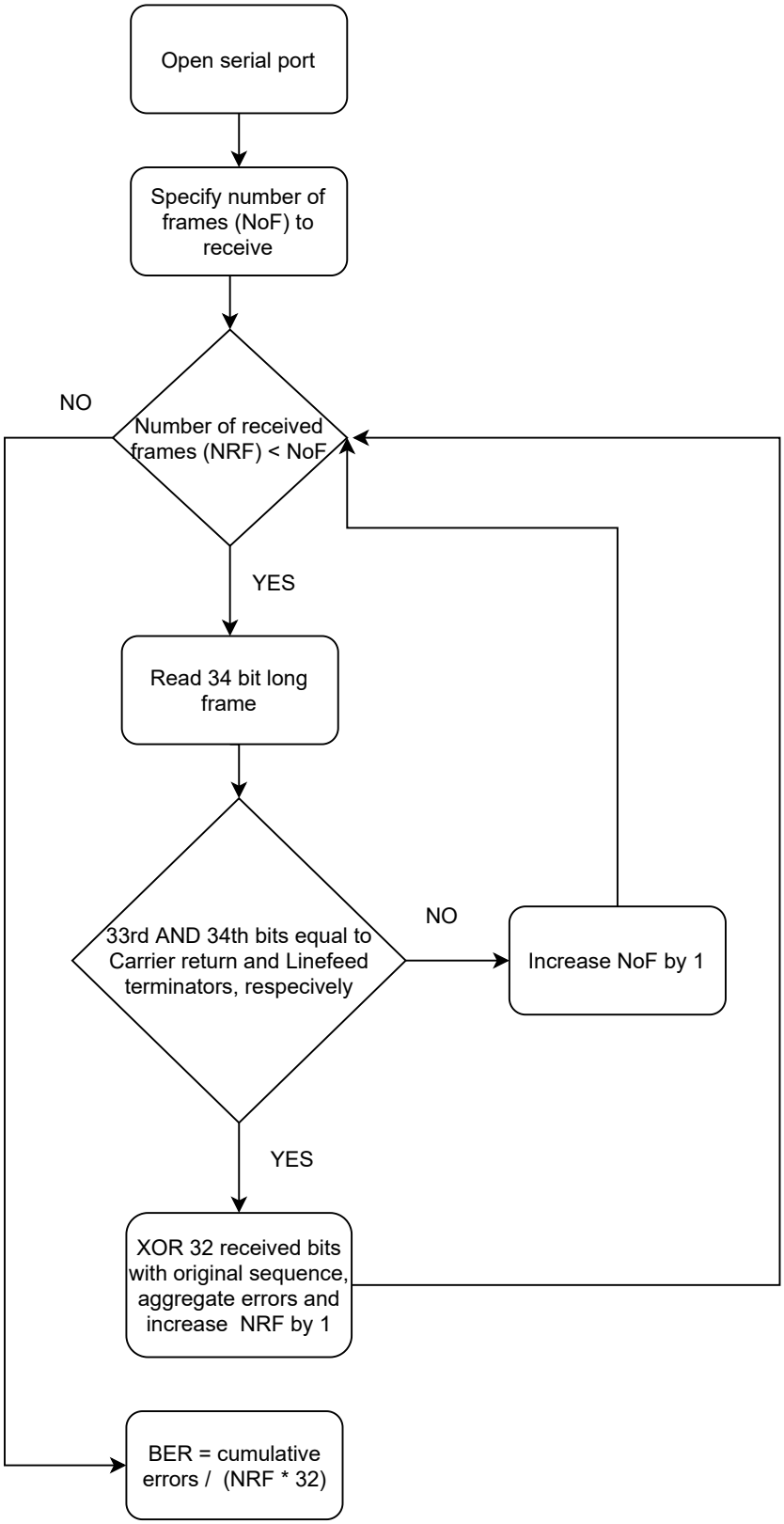

Figure 39. BER calculation algorithm.